



# Deforestation impacts on Amazon-Andes hydroclimatic connectivity

Juan Pablo Sierra<sup>1</sup> · Clementine Junquas<sup>1</sup> · Jhan Carlo Espinoza<sup>1</sup> · Hans Segura<sup>1</sup> · Thomas Condom<sup>1</sup> · Marcos Andrade<sup>2,3</sup> · Jorge Molina-Carpio<sup>2</sup> · Laura Ticona<sup>2</sup> · Valeria Mardoñez<sup>1,2</sup> · Luis Blacutt<sup>2</sup> · Jan Polcher<sup>4</sup> · Antoine Rabatel<sup>1</sup> · Jean Emmanuel Sicart<sup>1</sup>

Received: 6 June 2021 / Accepted: 21 October 2021 / Published online: 1 November 2021  
© The Author(s), under exclusive licence to Springer-Verlag GmbH Germany, part of Springer Nature 2021

## Abstract

Amazonian deforestation has accelerated during the last decade, threatening an ecosystem where almost one third of the regional rainfall is transpired by the local rainforest. Due to precipitation recycling, the southwestern Amazon, including the Amazon-Andes transition region, is particularly sensitive to forest loss. This study evaluates the impacts of Amazonian deforestation on the hydro-climatic connectivity between the Amazon and the eastern tropical Andes during the austral summer (December–January–February) in terms of hydrological and energetic balances. Using 10-years high-resolution simulations (2001–2011) with the Weather Research and Forecasting Model, we analyze control and deforestation scenario simulations. Regionally, deforestation leads to a reduction in the surface net radiation, evaporation, moisture convergence and precipitation (~20%) over the entire Amazon basin. In addition, during this season, deforestation increases the atmospheric subsidence over the southern Amazon and weakens the regional Hadley cell. Atmospheric stability increases over the western Amazon and the tropical Andes inhibiting convection in these areas. Consequently, major deforestation impacts are observed over the hydro-climate of the Amazon-Andes transition region. At local scale, nighttime precipitation decreases in Bolivian valleys (~20–30%) due to a strong reduction in the humidity transport from the Amazon plains towards the Andes linked to the South American low-level jet. Over these valleys, a weakening of the daytime upslope winds is caused by local deforestation, which reduces the turbulent fluxes at lowlands. These alterations in rainfall and atmospheric circulation could impact the rich Andean ecosystems and its tropical glaciers.

**Keywords** Deforestation · High-resolution climate modelling · Amazon basin · Amazon-Andes transition region · Energy and water balances

## 1 Introduction

The Amazon is the largest tropical rainforest in the world. It exchanges water, energy, and carbon with the atmosphere and is considered as an essential dynamic component of the climate system (Bonan 2008; Malhi et al. 2008). The Amazon ecosystem has been recognized as one of the major

sources of evapotranspiration (Fisher et al. 2011), releasing large amounts of water vapor to the atmosphere and sustaining rainfall not only in the Amazon itself, but also in remote regions of the South American continent (Eltahir and Bras 1994; Van Der Ent et al. 2010; Martinez and Dominguez 2014; Zemp et al. 2014). In addition, the latent heat release linked to moisture recycling over the Amazon basin engines global and regional atmospheric circulation (Gill 1980; Eltahir 1996; Gedney and Valdes 2000). Therefore, understanding the impacts of continued deforestation on the regional and global hydroclimate has become an urgent and extensively explored scientific question.

The Amazonian forest has been intensively cleared since the 1970's (Fearnside 1993; Nepstad et al. 2009). After a slowdown of deforestation rates during the period 2004–2012, the small-scale forest loss rates increased again over the last decade (Kalamandeen et al. 2018; Eiras-Barca

✉ Juan Pablo Sierra  
juan-pablo.sierra-perez@univ-grenoble-alpes.fr

<sup>1</sup> Institut des Géosciences de l'Environnement, Université Grenoble Alpes, IRD, CNRS, Grenoble, France

<sup>2</sup> Universidad Mayor de San Andrés, La Paz, Bolivia

<sup>3</sup> Department of Atmospheric and Oceanic Sciences, University of Maryland, College Park, USA

<sup>4</sup> Laboratoire de Météorologie Dynamique (LMD), CNRS-IPSL, École Polytechnique, Palaiseau, France

et al. 2020). Deforestation, as every effect of human activities on the climate system, disturbs the Earth's radiation budget and can be an important forcing for climate change (Hartmann et al. 2013; Mahowald et al. 2017). Indeed, when the rainforest is replaced by cropland or grassland, the energy balance is disturbed by: (i) a reduction in surface roughness and actual evapotranspiration, decreasing the surface energy loss from turbulent heat removal and latent heat flux (Gash and Nobre 1997; Lee et al. 2011; De Noblet-Ducoudré et al. 2012); (ii) an increase in the incoming solar radiation at the surface linked to less clouds and less evapotranspiration rates (Salati and Vose 1984; Bala et al. 2007); (iii) a reduction in absorbed solar radiation due to an increased surface albedo (Berbet and Costa 2003; von Randow et al. 2004); and finally (iv) less incoming infrared radiation driven by drier air as a result of the reduced evapotranspiration (Eltahir 1996; Claussen et al. 2001). *In-situ* measurements find a decrease in the surface net radiation over cleared areas (Bastable et al. 1993; von Randow et al. 2004). Although at the annual time scales an air temperature warming of the layer close to the surface follows the forest clearance (Gash and Nobre 1997), the reduction in the net surface radiation generates a cooling of the upper atmosphere and a subsidence that weakens the regional circulation (Eltahir 1996). In this sense, perturbations that initially occur at the surface and within the lower part of the atmosphere modify the vertical transport of heat and moisture, altering convection and subsidence over extended regions and affecting large-scale features such as the Hadley and Walker cells (Zhang et al. 1996; Snyder 2010; Badger and Dirmeyer 2015).

Atmospheric circulation and Amazonian rainforest compound a coupled bio-geophysical balanced system. Perturbations in the vegetation state through deforestation can drive very different changes in atmospheric circulation depending on its spatial scale. Observations and theoretical works show small-scale deforestation (< 10 km) triggering thermally driven land breeze resulting from differences in sensible heat fluxes between pastured and forested areas (Pielke 1984, 2001; Atkinson 1989; Wang et al. 1996; Souza et al. 2000; D'Almeida et al. 2007; Lawrence and Vandecar 2015). However, thermally driven circulations seem to be scale-dependent and can weaken as deforestation areas increase (Avisar and Schmidt 1998; Patton et al. 2005). At spatial scales larger than 100 km, land surface heterogeneities cannot produce enough surface gradient to sustain thermal circulation (Dalu and Pielke 1993). In fact, a recent study in Rondonia-Brazil demonstrates how when cleared areas grow, a shift occurs from a thermally convective regime towards a dynamically driven state where the roughness length reduction dominates and favors (inhibits) convection over areas in the downwind (upwind) direction of the deforested zone (Khanna et al.

2017). Since deforestation impacts on hydrological and atmospheric processes are complex and scale dependent, regional and global climate models stand out as useful tools to better understand the response of the climate system to land-use perturbations.

Numerical climate models have been extensively used for analyzing the impacts of deforestation over regional and global climate (Nobre et al. 2016 and references therein). Mesoscale models are able to represent the observed changes in circulation and clouds that follow small-scale deforestation (Chen and Avissar 1994; Wang et al. 2000; Saad et al. 2010). Furthermore, the thermal-to-dynamical shift regime caused by the rainforest loss reported over south-western Brazil is also reproduced by these models (Khanna et al. 2017). Under different deforestation scenarios, models project more frequent dry events and a lengthening of the Amazonian dry season (Nobre et al. 1991; Costa and Pires 2010; Bagley et al. 2014; Alves et al. 2017; Ruiz-Vásquez et al. 2020). Although recent observational studies report similar changes in Amazonian dry season hydrology since 1979, the attribution of these alterations to deforestation is not straightforward and evidence suggest an additional influence of the tropical north Atlantic Ocean warming (Fu and Li 2004; Yoon and Zeng 2010; Butt et al. 2011; Marengo et al. 2011; Fu et al. 2013; Debortoli et al. 2017; Espinoza et al. 2019, 2021; Leite-Filho et al. 2020). It is important to remark that, taking into account the dependency of climate response to the size of deforestation, the current spatial scale of Amazonian cleared area is not enough for predictions of extreme deforestation scenarios to be manifested or detected (D'Almeida et al. 2007; Nobre et al. 2016). On the other hand, under extensive deforestation scenarios climate models predict a reduction in precipitation recycling and rainfall in places downstream of the cleared areas caused by the shut off of forest transpiration (D'Almeida et al. 2007; Moore et al. 2007; Correia et al. 2008; Swann et al. 2015). At the same time, empirical estimates have found that south-western Amazon is particularly dependent on evapotranspiration from other parts of the basin (Zemp et al. 2017b; Staal et al. 2018). Hence, several simplified and regional climate models present a decrease in rainfall and moisture transport over this particular area (Sun and Barros 2015a; Boers et al. 2017; Zemp et al. 2017a; Ruiz-Vásquez et al. 2020). However, an opposite effect of intensified moisture transport towards south-western Amazon and south-eastern South America has been suggested by some modelling studies as the result of deforestation induced decreasing in surface roughness (Lean and Rowntree 1997; Eiras-Barca et al. 2020). These different responses to similar deforestation scenarios suggest the need to further assess the impacts of Amazon forest clearance over the regional climate.

In the Amazon-Andes transition region lies the rainiest and biologically richest area of the entire Amazon basin

(Myers et al. 2000; Killeen et al. 2007; Hoorn et al. 2010; Espinoza et al. 2015). This region encompasses complex Andean topography, ranging between almost sea level in the Amazon lowlands to more than 6000 m a.s.l. over the Andean summits. This causes a strong orographic effect that interacts with regional atmospheric circulation to produce an exceptional spatial rainfall contrast (Chavez and Takahashi 2017; Junquas et al. 2018). There, high precipitation rates lead to large values of runoff per unit area (Moquet et al. 2011), providing most of the sediment load to Amazon rivers (Vauchel et al. 2017; Armijos et al. 2020). Consequently, extreme hydrological events over this region can impact the whole basin downstream (Espinoza et al. 2014). Particularly, the Amazon-Andes transition region exhibits the largest precipitation recycling (portion of the precipitated water previously transpired by the Amazonian rainforest) of the Amazon catchment (Eltahir and Bras 1994; Dirmeyer and Brubaker 2007; Van Der Ent et al. 2010; Staal et al. 2018). Therefore, this region can potentially be highly sensitive to Amazon deforestation effects. Nevertheless, the surface-atmosphere coupling over this area has been poorly studied and most of the referent work has been focused over Brazilian Amazon or was based on coarse horizontal resolution modelling experiments insufficient to capture the required details of the topographical influence on local convection.

This study aims to better understand the deforestation effects on moisture transport and rainfall over the Amazon-Andes transition region during the heart of the wet season (December–January–February, DJF). During this season nearly 50% of total annual precipitation falls over the region (Espinoza et al. 2009). Since Amazonian groundwater recharge during wet periods can sustain forest transpiration rates during dry months (Miguez-Macho and Fan 2012), DJF alterations in rainfall patterns may have a profound impact in the watershed hydrology. The strong summer convection in the region is controlled by atmospheric processes that are part of the development of the South American Monsoon System (SAMS; Vera et al. 2006; see Sect. 3.1 for details) and which may be sensitive to impacts on surface energy/water fluxes induced by land use change (Li and Fu 2004).

Taking into account the potential sensitivity of the Amazon-Andes transition region to deforestation and the need for high-resolution studies, the present work analyzes the deforestation land-use change impacts on regional energy and water budgets, as well as rainfall alterations at a local scale through the use of high-resolution simulations (up to 1 km horizontal grid size) with the regional climate model Weather Research and Forecasting Model (WRF). Model hourly outputs are compared with observational data from rain-gauges and satellites in order to elucidate the possible changes caused by Amazonian deforestation in the diurnal and nocturnal precipitation inside two typical Andean valleys during 2001–2011 austral summers. We describe the

configuration of the model, the deforestation experiment and reference data used in Sect. 2. In Sect. 3, we validate the model skill to reproduce the precipitation, general circulation and moisture transport at regional scale, as well as its ability to properly represent the deforestation signal in comparison with observations from the Large-Scale Biosphere–Atmosphere (LBA) project. The impacts of deforestation on moisture transport and rainfall at regional, meso and local scales are analyzed in Sect. 4. Finally, Sect. 5 summarizes and discusses the main results.

## 2 Data and methods

### 2.1 Model description

This study uses the regional climate model WRF version 4.1 (Skamarock et al. 2019). The model WRF was used in previous works to study the climatology of tropical South America and the Amazon basin (Bagley et al. 2014; Sun and Barros 2015b, a; Mourre et al. 2016; Junquas et al. 2018; Spera et al. 2018; Trachte 2018; Heredia et al. 2018; Yang and Dominguez 2019; Eiras-Barca et al. 2020; Saavedra et al. 2020). WRF is a non-hydrostatic model with terrain-following vertical levels (we use 49 vertical levels with higher level density near the surface). We employ three one-way nested modelling domains as shown in Fig. 1a. Table 1 summarizes the information of spatial and temporal resolution for each of the three domains used in this work. The first domain encompasses tropical South America and has a horizontal resolution of 15 km × 15 km with a time step of 90 s. The second and third domains have spatial resolutions of 5 km × 5 km and 1 km × 1 km, respectively and cover the south-western part of the basin. Time steps for these two domains are 30 s and 6 s, respectively. Domain 3 comprises the instrumented Andean valleys of Zongo and Huarinilla used for model validation (Fig. 1b). In order to analyze the diurnal and nocturnal atmospheric conditions we use an output time resolution of 3 h for domains 1 and 2, and 1 h for the finest domain.

Lateral boundary conditions from ERA5 reanalysis (Hersbach et al. 2020) are used. This reanalysis presents an enhanced horizontal resolution of 0.28° × 0.28° (31 km) with data available every 6 h (<https://www.ecmwf.int/en/forecasts/datasets/reanalysis-datasets/era5>). Significant improvements in the representation of several model processes in this reanalysis are reflected in a better fit in winds, temperature and humidity in the troposphere compared against radiosonde data (Hersbach et al. 2020).

Preliminary tests for different model configurations (not shown) allow selecting the parameterizations shown in Table 2. Summarizing, we use the Yonsei University scheme for representation of the boundary layer (Hong et al. 2006)

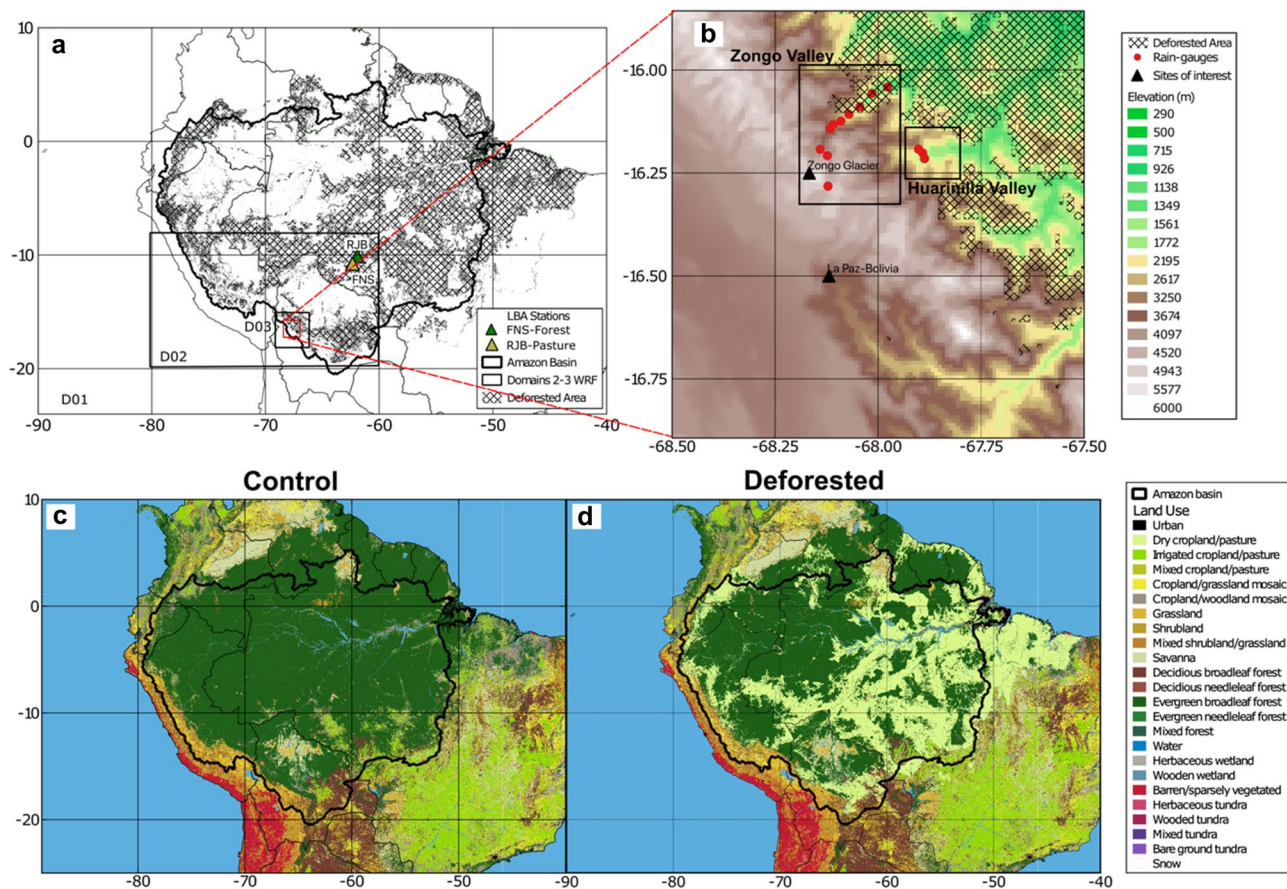


**Fig. 1** **a** WRF simulation domains (black boxes labelled D01, D02, and D03 respectively), deforested area and locations of selected flux towers from the Large-Scale Biosphere–Atmosphere Experiment in the Amazon. Domains 1, 2 and 3 encompass the areas 24 °S–10 °N/90–40 °W, 20–8 °S/80–60 °W and 18–15 °S/69–66 °W

respectively. Delineated area represents the boundary of the Amazon River basin (black). **b** D03 subregion (red square in **a**) and locations of rain-gauges stations over two Andean mountain valleys. Land-use category distributions for: **c** Control and **d** deforested scenarios

**Table 1** Characteristics of the domains used in WRF simulations

	WRF-D01	WRF-D02	WRF-D03
Horizontal resolution (km)	15	5	1
Domain	Tropical South America	South-western Amazon	Bolivian Andean valleys
Domain center coordinates	7° 30' 00" S, 65° 00' 00" W	13° 56' 12" S, 70° 4' 49" W	16° 35' 49" S, 67° 38' 56" W
Configuration	Regional simulation	One-way nesting	One-way nesting
Forcing	ERA5	WRF-D01	WRF-D02
Vertical resolution	49 hybrid vertical levels	49 hybrid vertical levels	49 hybrid vertical levels
Run time step (s)	90	30	6
Output time resolution (h)	3	3	1

with the wind topographic correction activated (Jiménez and Dudhia 2012). This wind correction takes into account the momentum sink term generated by the unresolved terrain at sub-grid scale in the model. It has shown improvements in the simulated wind field over complex terrains (Jiménez and Dudhia 2012) and has already been tested in the tropical

Andes (Junquas et al. 2018). Lin’s microphysics scheme is implemented (Lin et al. 1983) for phase change and precipitation. We also use Grell 3D parametrization for sub-grid scale convection over domains 1 and 2 (Grell and Dévényi 2002). Previous studies demonstrate convection parametrizations as one of the major uncertainties in the representation

**Table 2** Physical parameterizations used in WRF simulations

	Parameterizations	References
Radiation	Longwave: rapid radiative transfer model (RRTM)	Mlawer et al. (1997)
	Shortwave: Dudhia scheme	Dudhia (1989)
Cumulus	Grell 3D	Grell and Dévényi (2002)
Planetary boundary layer	Yonsei University scheme	Hong et al. (2006)
Land surface	Noah land surface model	Chen and Dudhia (2001)
Cloud microphysics	Lin scheme	Lin et al. (1983)
Surface layer	MM5 similarity	Paulson (1970)

of rainfall diurnal cycle (Brockhaus et al. 2008; Hohenegger et al. 2008). Taking this into account and considering that a spatial resolution higher than 4 km is considered enough for non-hydrostatic models to explicitly solve convection (Weisman et al. 1997; Ramos da Silva and Avissar 2006), we deactivate the cumulus parameterization over the finest domain. Additionally, we change the default WRF topography from the United States Geological Survey (USGS) to the Shuttle Radar Topography Mission (SRTM) product (Farr et al. 2007). This dataset presents a more realistic representation of the altitude of meteorological stations over the Peruvian Andes when compared with USGS and enhances the representation of rainfall and temperature in the same region with the model WRF (Saavedra et al. 2020). The SRTM dataset has a spatial resolution of 30 arc-second or approximately 1 km.

In order to obtain a climatological state of the south-western Amazon wet season, our simulations cover 10 years of austral summers for the time period 2001–2011. Each simulation starts on November 1st and the first month is removed as a spin-up for the output analysis.

## 2.2 Description of the experiments

For each austral summer in the period 2001–2011, we conduct two simulations with WRF sharing the same atmospheric lateral boundary conditions, but with different land-cover states. The control simulation (“Control” or “Con”) corresponds to vegetation conditions for the year 2000 using the land cover map developed for South America by Eva et al. (2004) (Fig. 1c). This dataset was implemented in WRF by Saavedra et al. (2020) and exhibits a spatial resolution of 1 km × 1 km. For the deforested simulation (“Deforested” or “Def”), we use the deforested scenario 2050 business-as-usual from Soares-Filho et al. (2006; Fig. 1d). This scenario reaches 45% of forest lost and assumes the continuation of the 1997–2002 registered deforestation rates, no definition of new protected areas in the basin and the building of all planned highways (Soares-Filho et al. 2006). This scenario does not include the forest impoverishment through logging and fires. The implemented deforestation polygon is shown

in Fig. 1a. Amazon deforestation involves the replacement of native forest by mixed crops (mainly soybean and corn), as well as pasture for cattle feeding. For this reason, within the deforested polygon natural vegetation (this includes all types of forest, shrublands, grasslands and savannas) grid points are replaced by cropland/grassland mosaics.

## 2.3 Data

In order to validate the model’s ability to represent the rainfall spatial distribution in the region, we use the product Tropical Rainfall Measuring Mission 3B42 (TRMM; <https://disc.gsfc.nasa.gov>). This dataset, available from 1998, presents a 0.25° × 0.25° resolution and includes precipitation rates every 3 h (Huffman et al. 2007). However, previous studies have identified a strong rainfall underestimation by TRMM in the Amazon-Andes region (Espinoza et al. 2015; Zubieta et al. 2015; Chavez and Takahashi 2017). For this reason, we complement the model validation with daily information of 10 rain-gauge stations (Fig. 1b) from the Bolivian Electric Power Company (COBEE) and managed in collaboration with the Institute of Research for the Development (IRD)—France. Additionally, three stations with hourly data were used from Schwabe et al. (2011). Table 3 presents the general information of each rain-gauge station according to official records of COBEE. We complement this information with location and altitude information of the stations from author’s field campaigns (Table S1). The quality assessment of these rainfall stations was carried out by previous works (Molina-Carpio et al. 2019 and Laura Ticona, personal communication). The use of in-situ information also allows characterizing the model skill to capture the precipitation variability at small spatial scale in an Andean valley where local processes are important (Egger et al. 2005; Trachte et al. 2010; Junquas et al. 2018). Additionally, the representation of the regional atmospheric circulation and moisture transport are validated by a direct comparison between WRF outputs and ERA5 and NCEP-NCAR (Kalnay et al. 1996) data.

To test whether WRF responds realistically to the changes induced by land-use alterations, we use observations of

**Table 3** Name, geographic location, elevation, temporal range and annual rainfall of rain-gauge stations from the Bolivian Electric Power Company (COBEE) and Schawe et al. (2011)

Name of station	Location (latitude, longitude)	Elevation (m a.s.l.)	Temporal period (years)	Mean annual rainfall and standard deviation in mm/year (mean and standard deviation of DJF rainfall in mm/month)
Plataforma	16° 16' 43.0" S, 68° 07' 24.0" W	4750	1971–2018	691 ± 221 (138 ± 23)
Tiquimani	16° 12' 27.1" S, 68° 07' 20.0" W	3900	1971–2018	918 ± 274 (196 ± 33)
Botijlaca	16° 11' 32.5" S, 68° 08' 26.0" W	3492	1971–2018	983 ± 128 (178 ± 35)
Cuticucho	16° 08' 34.5" S, 68° 06' 55.0" W	2697	1971–2018	2053 ± 180 (341 ± 50)
Santa Rosa	16° 07' 55.8" S, 68° 06' 29.5" W	2505	1971–2018	1748 ± 563 (317 ± 51)
Sainani	16° 07' 24.5" S, 68° 05' 21.5" W	2210	1971–2018	1975 ± 604 (358 ± 46)
Chururaqui	16° 06' 20.7" S, 68° 04' 05.5" W	1830	1971–2018	2086 ± 211 (334 ± 67)
Harca	16° 05' 20.2" S, 68° 02' 40.0" W	1480	1971–2018	2061 ± 678 (358 ± 73)
Cahua	16° 03' 21.6" S, 68° 00' 50.7" W	1195	1981–2018	2595 ± 394 (405 ± 76)
Huaji	16° 02' 28.4" S, 67° 58' 37.4" W	945	1999–2018	2676 ± 830 (454 ± 70)
Hornuni 1800	16.215° S, 67.887° W	1800	2001–2002	2310 (311)
Hornuni 2600	16.201° S, 67.892° W	2600	2001–2002	3970 (489)
Hornuni 3010	16.192° S, 67.902° W	3010	2001–2002	5150 (651)

Annual and DJF rainfall means in the fifth column correspond to the period 2001–2011 except for the three last stations covering the period 2001–2002. Geographic location and elevation of rain-gauge stations recorded by author's field campaigns are shown in Supplementary material, Table S1

energy surface fluxes, air temperature, precipitation and wind speed from the Large-Scale Biosphere–Atmosphere (LBA) project (Saleska et al. 2013). This dataset is available at the website [https://daac.ornl.gov/LBA/guides/CD32\\_Brazil\\_Flux\\_Network.html](https://daac.ornl.gov/LBA/guides/CD32_Brazil_Flux_Network.html). The LBA project was a large scientific effort carried out between 1996 and 2006 for assessing the influence of tropical forest conversion in carbon storage, nutrient dynamics and trace gas fluxes in the Amazon. Since the region of interest of this study is the Amazon-Andes transition region, we only use the closest stations from the LBA project that fits inside our second modelling domain (Fig. 1a). Because of their geographical location, these stations experience annual cycles of precipitation and temperature similar to the south-western Amazon variability. The first station, *Fazenda Nossa Senhora de Aparecida* (yellow triangle labeled as “FNS” in Fig. 1a), is a cattle ranch located at the center of a deforested area of about 50 km in radius cleared in 1977 for crop cultivation. The tower flux stands at 306 m a.s.l., 10.75° S, 62.35° W and presents daily data for the period 1999–2002. The second station corresponds to *Rondonia Jaru Biological Reserve* and is located at 191 m a.s.l., 10.08° S, 61.93° W (green triangle labeled as “RJB” in Fig. 1a). This is a natural reserve of the Brazilian Environmental Protection Agency covered by tropical dry forest with a mean tree height of 33 m that was established in the 1960s and expanded in 2006. The proximity of these stations (around 87 km) allows testing the impacts of land use change on surface fluxes and the atmospheric bottom conditions. For validation we only use

data for DJF 2001–2002 when WRF simulations and LBA data availability periods overlap in time.

## 2.4 Calculation of energy/water balances and atmospheric stability

The energy budget at the surface is described by Duveiller et al. (2018):

$$N_R = (S_{in} - S_{out}) + (L_{in} - L_{out}) = Sens_H + Lat_H + Gr_H \quad (1)$$

Here,  $N_R$  corresponds to net radiation and is the summation of contributions from shortwave and longwave components:  $S_{in}$  is the incident shortwave or solar radiation,  $S_{out}$  is the reflected solar radiation,  $L_{in}$  is the incoming longwave component and  $L_{out}$  is the emitted longwave radiation flux. The net turbulent heat flux is later distributed in sensible heat flux ( $Sens_H$ ), latent heat flux associated with evaporation from the surface ( $Lat_H$ ) and molecular conduction flux from the ground ( $Gr_H$ ). All the terms in Eq. (1) are in  $W/m^2$ . Land use change disturbances in the energy budget are assessed by computing the differences in DJF climatological means for each term of Eq. (1) between Deforested and Control scenarios.

The atmospheric water budget establishes how precipitation, evapotranspiration and net moisture transport entering/leaving an atmospheric column controls the temporal changes in the vertically integrated water content (Peixoto and Oort 1992). At seasonal timescales the temporal changes in atmospheric moisture are negligible and precipitation,

evapotranspiration and column moisture convergence nearly balances each other (Brubaker et al. 1993; Li et al. 2013). Hence, the climatological changes induced by deforestation in the water balance can be expressed as follows:

$$\Delta \bar{P}_{Def-Con} = \Delta \bar{E}_{Def-Con} - \frac{1}{g} \Delta \nabla \cdot \int_{1000_{hPa}}^{200_{hPa}} q \bar{\mathbf{V}}_H dp \quad (2)$$

In Eq. (2),  $P$  is precipitation,  $E$  is evapotranspiration and  $\nabla \cdot \int_{1000_{hPa}}^{200_{hPa}} q \bar{\mathbf{V}}_H dp$  is the divergence field of vertically integrated moisture flux from 1000 to 200 hPa. The bars denote climatological DJF means.

Finally, we evaluate the deforestation impacts on the atmospheric stability in tropical South America. Over the Amazon, the moistening of mid-tropospheric levels is associated with the development of deep convection in the region, which is related to the decreasing of atmospheric stability between middle and upper levels of the troposphere (Scala et al. 1990; Zhuang et al. 2017). For this reason, recent works use the difference of equivalent potential temperature ( $\theta_e$ ) between middle (500 hPa) and upper (200 hPa) troposphere ( $\theta_{e_{200-500}}$ ) as an atmospheric stability index (Segura et al. 2020). The equation of equivalent potential temperature can be written following Stull and Ahrens (2011):

$$\theta_e = \theta + \left( \frac{L_V \theta}{C_p T} \right) r \quad (3)$$

where,  $\theta$  corresponds to potential temperature,  $L_V$  is the latent heat of vaporization,  $C_p$  is the specific heat for air at constant pressure,  $T$  corresponds to the air absolute temperature and  $r$  is the air mixing ratio. The first term of this equation is related to dry adiabatic processes while the second one includes the effect of moisture in the net energy of an air parcel. Thus, the changes in the difference between mid and upper tropospheric equivalent potential temperature ( $\theta_{e_{200-500}}$ ) allows separating the individual effects of dry and wet processes in the regional atmospheric stability. Again, climatological mean differences in each term of Eq. (3) between Deforested and Control scenarios allow evaluating the impact of deforestation in the regional atmospheric stability.

### 3 Model validation

#### 3.1 Regional scale

The development of the SAMS establishes a northerly cross-equatorial flow (Wang and Fu 2002) and enhances convection over central Amazon (Vera et al. 2006; Fig. 2a, c). A cloudiness/rainfall band known as the South Atlantic

Convergence Zone (SACZ) extends from southern Amazonia towards south-eastern Brazil and accompanies the mature phase of the SAMS (Kodama 1992; Figueroa et al. 1995; Zhou and Lau 1998; Fig. 2a). The diabatic heating released by the convective activity generates a large anticyclonic circulation at the upper troposphere centered around 15 °S–65 °W known as the Bolivian High (Lenters and Cook 1997; Fig. 2e). Latent heat release over central Amazon also promotes a low-level continental-scale gyre that transports water vapor from the Atlantic Ocean inland towards Amazon and La Plata basins (Rodwell and Hoskins 2001; Vera et al. 2006; Fig. 2c). Over the eastern flank of the Andes, this circulation reaches its maximum wind velocities forming the South American Low-Level Jet (SALLJ). Over its trajectory, the transport of moisture through the SALLJ encounters the topographical barrier of the Andes triggering forced convection in very localized places or rainy hotspots mainly in the Bolivian and Peruvian piedmonts (Espinoza Villar et al. 2009; Espinoza et al. 2015; Chavez and Takahashi 2017; Fig. 2a).

In general terms, the model is able to reproduce the main precipitation features during the austral summer (Fig. 2b). WRF-D01 represents the strong precipitation over central Amazon but with its maximum shifted eastward. The characteristic northwest-southeast rainfall band of the SACZ is present in WRF simulation. However, the model shows a considerable negative bias over the northern Peruvian lowlands (until – 50% of dry bias when compared to TRMM; red contours in Fig. 2b). Rainfall Peruvian and Bolivian hotspots are also part of the model climatology. Nevertheless, WRF underestimates the former and overestimates the latter. The Atlantic ITCZ is strongly overestimated by WRF (up to + 200% with respect to TRMM; red contours in Fig. 2b). This wet bias is related to a too strong vertically integrated moisture convergence in the model output (Fig. 2d). Finally, upper and lower atmospheric circulations are realistically represented by WRF (Fig. 2d, f). As in ERA5 outputs, WRF easterly low-level winds carry moisture from the Atlantic Ocean toward the continent (Fig. 2d). The moisture flow moves parallel to the Andes cordillera mechanically deviated exporting humidity toward southern latitudes both for ERA5 and WRF. At the altitude of 200 hPa, the model develops the anticyclonic circulation of the Bolivian High (Fig. 2f). Similar features of vertically integrated moisture flux and upper level atmospheric circulation are found in NCEP-NCAR reanalysis (see Supplementary material, Fig. S1).

#### 3.2 Local scale

In order to validate if WRF reproduces the observed land use change impacts on surface fluxes and atmospheric variables at a local scale, we compare the selected LBA stations (Sect. 2.3) against the WRF-D02 Control simulation for

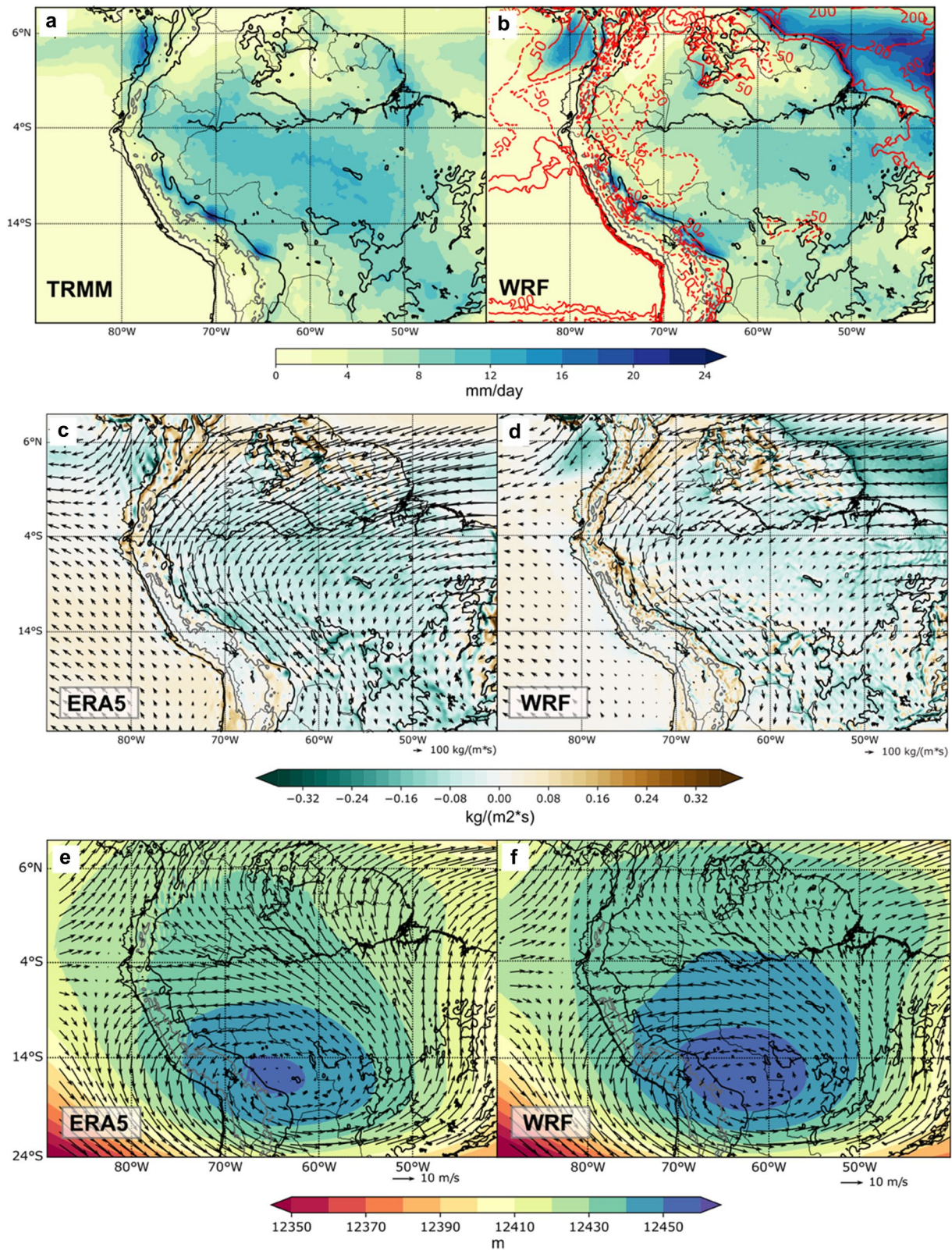


**Fig. 2** DJF climatological means over the period 2001–2011 for: **a** and **b** precipitation from TRMM-3B42 (**a**) and WRF-Control (**b**) in mm/day. Red lines in **b** represent rainfall differences with respect to TRMM in percentage. **c** and **d** vertically integrated moisture flux (vectors, kg/m<sup>2</sup>s) and its divergence (shaded, kg/m<sup>2</sup>s) from ERA5

(**c**) and WRF-Control (**d**). **e** and **f** horizontal winds (vectors, m/s) and geopotential height (shaded, m) at 200 hPa from ERA5 (**e**) and WRF-Control (**f**). Orography elevation is shown at 500 and 3500 m a.s.l. as black and grey contours, respectively



DJF 2001–2002. We take the paired pasture/rainforest sites from the LBA project and compute the observed changes in surface variables in percentage respect to the forest values. Then, similarly, we take the coordinates of the LBA pasture and rainforest stations and extract information of atmospheric variables from model outputs in order to compute the percentage changes. For WRF outputs, we average variables of interest around each location inside a surrounding area of  $15 \text{ km} \times 15 \text{ km}$  (one grid-point-radius) but selecting only the grids corresponding to cropland/grassland or forest respectively and ignoring grid cells with a different land use category. Between a 15 km radius and a 50 km radius, no significant changes are found in the WRF deforestation response (not shown).

Figure 3 shows the simulated and observed (orange and blue bars, respectively) mean differences of surface variables due to deforestation. Significant differences are highlighted in red contour according to a  $t$ -test ( $p < 0.05$ ). In general terms, WRF is able to properly represent the nature of most of the alterations in surface fluxes and atmospheric variables induced by the land use change. Land cover change is related to reduced precipitation by around  $-44\%$  and  $-30\%$  in observations and WRF, respectively. However, since precipitation is also related with non-local processes, it is difficult to establish a deforestation-rainfall causality relation. Consistently, significant reductions in surface specific humidity are observed but weakly simulated (around  $-11\%$  and  $-1\%$  in observations and WRF, respectively).

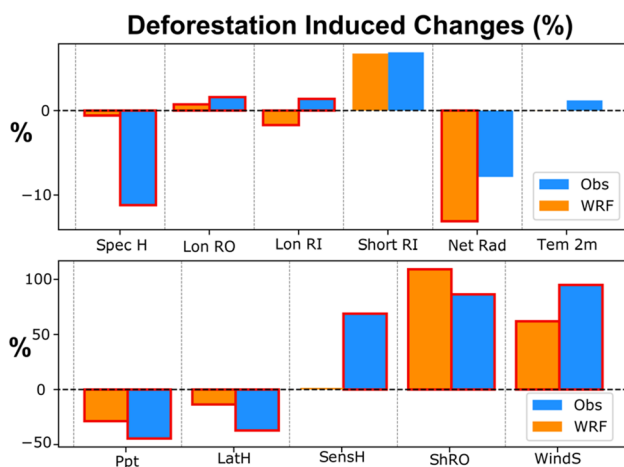


**Fig. 3** Deforestation induced changes in surface atmospheric variables over LBA stations (blue bars) and WRF-D02 (orange bars) for DJF in the period 2001–2002. Significant differences are delineated in red ( $t$ -test,  $p < 0.05$ ). Abbreviations are as follows: Spec H—specific humidity at 2 m, Lon RO—longwave outgoing radiation, Lon RI—longwave incoming radiation, Short RO—shortwave outgoing radiation, Short RI—shortwave incoming radiation, Net-Rad—net radiation, Tem2 2 m—air temperature at 2 m, LatH—latent heat flux, SensH—sensible heat flux, Ppt—precipitation, WindS—wind speed at 10 m

Accordingly, there is a significant decrease in latent heat flux for observations ( $-37\%$ ) with a weaker response by WRF ( $-14\%$ ). This implies that WRF underestimates the evapotranspiration response induced by deforestation. There is a significant increase in sensible heat flux and surface air temperature in LBA stations ( $68\%$  and  $1\%$ , respectively). WRF strongly underestimates the sensible heat increase and even slightly invert the temperature response to land use change ( $1.49\%$  and  $-0.02\%$  respectively). The effects of the increased sensible heat and temperature (only sensible heat in WRF) act to give an increase in the outgoing longwave radiation flux in LBA stations of  $1.6\%$  ( $0.7\%$  in WRF). Since pastures and croplands are brighter than forest (Oguntoyinbo 1970; Bonan 2008), an increase in the albedo raises the outgoing or reflected shortwave radiation by  $86\%$  for observations (Loarie et al. 2011). The albedo effect is overestimated by WRF, which presents an outgoing shortwave radiation pasture/forest difference of  $104\%$ . This overestimated energy loss can be related with the model underestimation of sensible heat flux increase. More incoming shortwave radiation reaches the surface in model and observations ( $4\%$  and  $7\%$  respectively). This difference in WRF simulation is a consequence of cloud reduction over deforested areas (not shown). There is a disagreement between the modelled and observed changes in the incoming longwave radiation. While WRF exhibits a decrease in this variable ( $-1.64\%$ ), observations report an increase of about  $1.38\%$ . This difference is possibly explained by biases in the model representation of clouds or because of the drier WRF mid-upper troposphere (not shown). At the end, driven by the incremented energy losses through longwave radiation fluxes and shortwave radiation reflection, there is a reduction in net radiation for WRF ( $-15\%$ ) and LBA stations ( $-8\%$ ). Finally, the enhanced surface wind speed at 2 m is a direct consequence of the deforestation induced roughness-length reduction in both model ( $53\%$ ) and observations ( $95\%$ ).

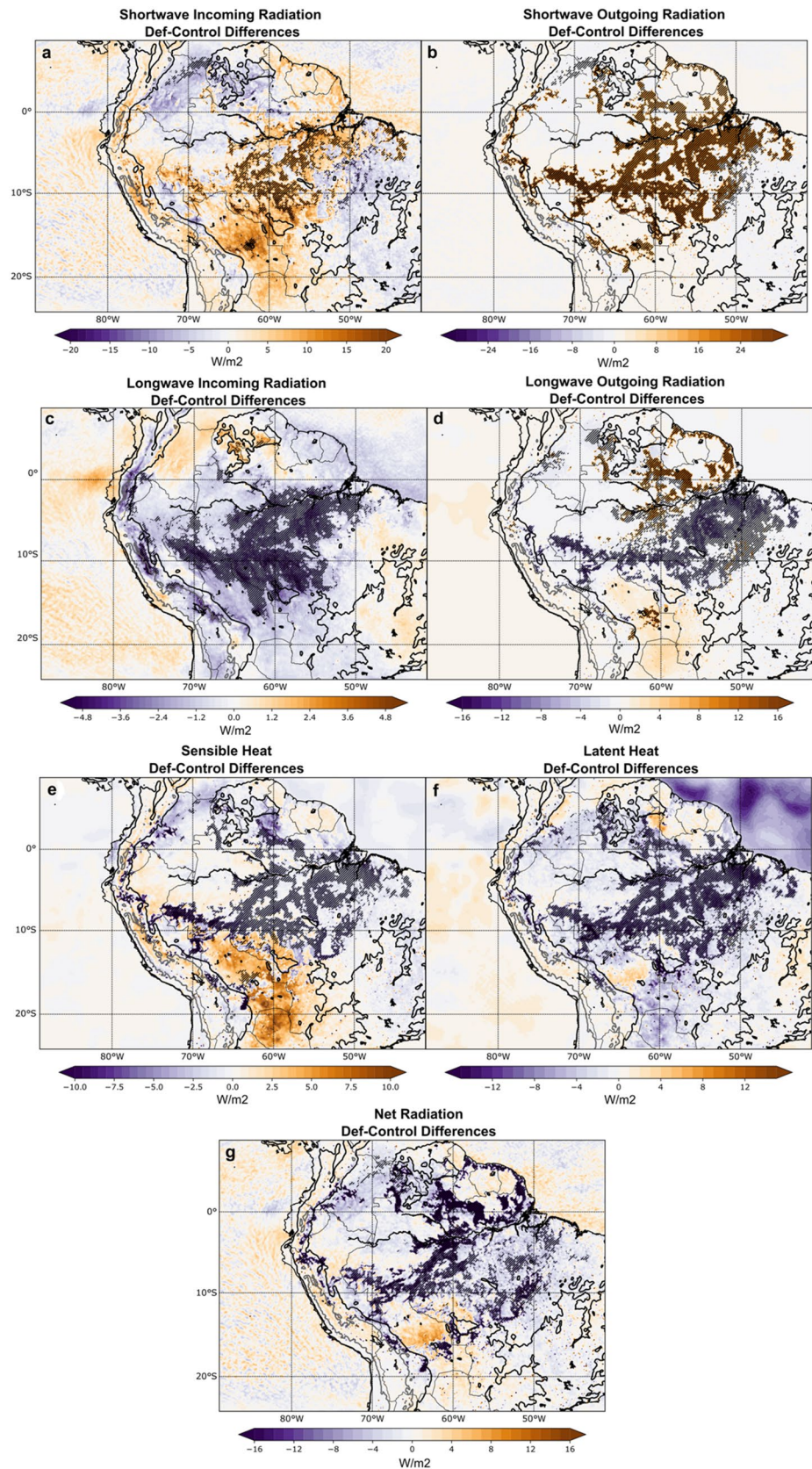
## 4 Results and discussion

This section is composed of two subsections, in the first part we evaluate the effects of deforestation in the energy and water balances, as well as the atmospheric stability at regional-scale ( $90^\circ$ – $60^\circ$  W,  $24^\circ$  S– $9^\circ$  N). The second subsection is focused on the alterations in the hydro-climatology at meso and local scales, especially over the Amazon-Andes transition region and Andean valleys of Bolivia.

### 4.1 Regional changes in energy and water balances

Climatological alterations in the surface energy balance (Eq. 1) induced by deforestation are shown in Fig. 4, in which significant differences are highlighted with black

**Fig. 4** DJF seasonal climatological differences Deforsted minus Control during 2001–2011 in surface energy balance variables: **a** Shortwave incoming radiation ( $\Delta \overline{S_{in}^{Def-Con}}$ ). **b** Shortwave outgoing radiation ( $\Delta \overline{S_{out}^{Def-Con}}$ ). **c** Longwave incoming radiation ( $\Delta \overline{L_{in}^{Def-Con}}$ ). **d** Longwave outgoing radiation ( $\Delta \overline{L_{out}^{Def-Con}}$ ). **e** Sensible heat flux ( $\Delta \overline{Sens_H^{Def-Con}}$ ). **f** Latent heat flux ( $\Delta \overline{Lat_H^{Def-Con}}$ ). **g** Net radiation ( $\Delta \overline{NR_{Def-Con}}$ ). All figures are in  $W/m^2$ . Significant changes (t-test,  $p < 0.05$ ) are marked with black slashes. Orography elevation is shown at 500 and 3500 m a.s.l. as black and grey contours, respectively



slashes. The last term in Eq. 1 corresponding to soil heat flux is omitted because it exhibits much smaller magnitudes with respect to the other terms ( $\pm 1 \text{ W/m}^2$ ). Indeed, in situ measurements report low soil heat fluxes below tropical forest (Shuttleworth et al. 1984), but important values for crops (Oliver et al. 1987; Gash and Shuttleworth 1991).

Important changes in the incoming solar radiation are induced by the forest loss in the region (Fig. 4a). In general, more (less) incident solar radiation reaches the ground over places where reduction (rise) in precipitation and moisture convergence are located (see Fig. 5) such as in the central and south-western Amazon (north of South America and eastern Brazil). Hence, disturbances in incident solar radiation are closely linked with changes in clouds in WRF simulations as confirmed by analyzing top of the atmosphere (TOA) outgoing longwave flux and cloud water content (not shown). However, major changes in the energy balance occur in the outgoing shortwave radiation (Fig. 4b). A significant increase in about  $+20 \text{ W/m}^2$  occurs only over

deforested areas which reflects the very local response induced by the higher cropland/grassland albedo. With a minor response, reductions in the longwave incoming radiation occur over most of the Amazonian watershed (Fig. 4c) as a result of a drier atmosphere and lower cloud cover in the deforested scenario (not shown). On the other hand, there is a meridional dipole in longwave outgoing radiation changes (Fig. 4d). Important disturbances in this variable take place mainly over deforested areas which implies the influence of very local processes. North of the Amazon river ( $< 5^\circ\text{S}$ ) at the East of the basin, upward longwave radiation increases as a consequence of an increase in surface emissivity over this area (not shown). However, in the southern part of the basin, less outgoing longwave radiation is related to reductions in the air surface temperature. Sensible heat disturbances are linked to surface air temperature changes (not shown). Thereby, reductions (increments) in this turbulent flux are located over deforested areas (Fig. 4e) and are related to decreasing (increasing) surface temperature (not

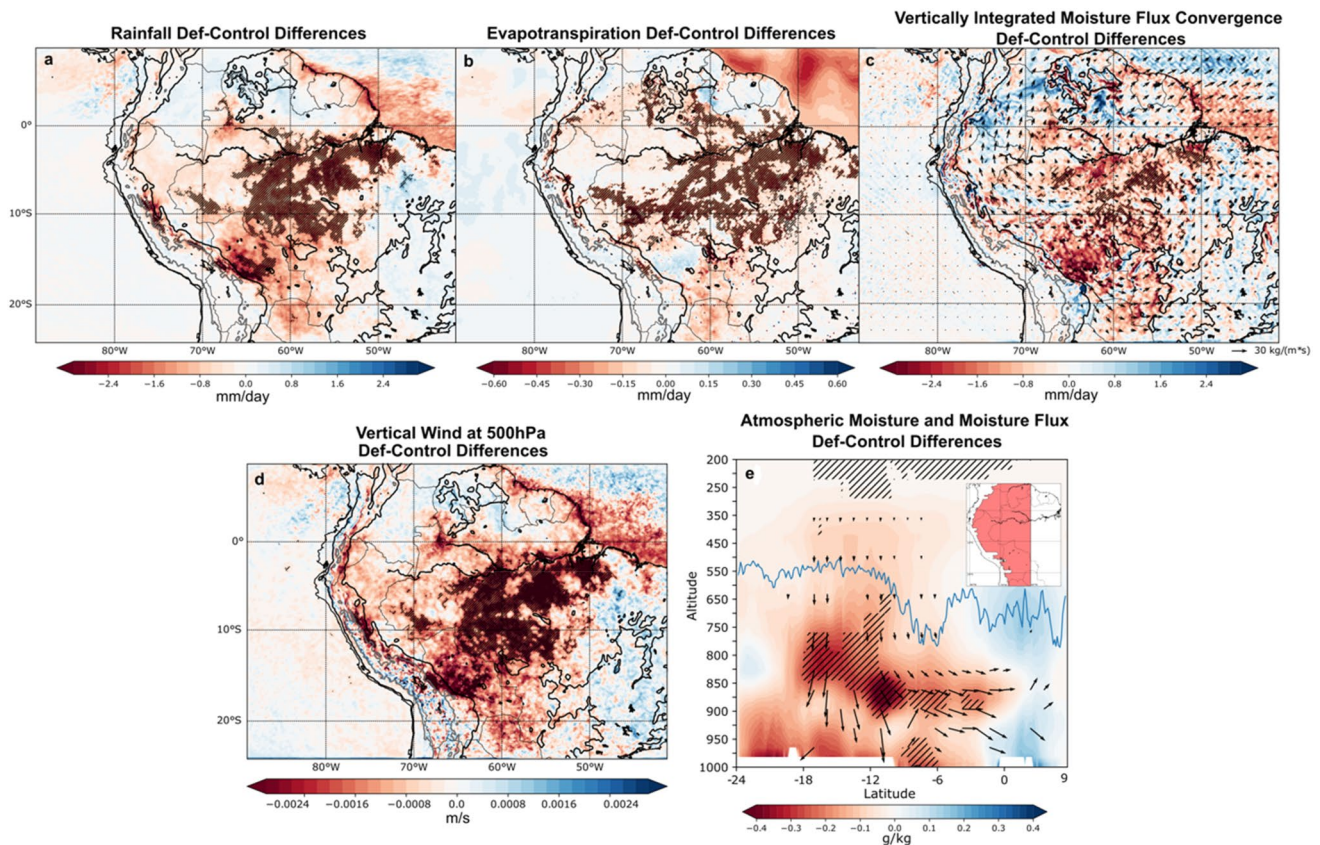


**Fig. 5** DJF seasonal climatological differences Deforested minus Control during 2001–2011 in water balance variables: **a** Rainfall ( $\Delta P_{Def-Con}$ ). **b** Evapotranspiration ( $\Delta E_{Def-Con}$ ). **c** Vertically integrated moisture flux (vectors) and moisture flux convergence ( $-\frac{1}{g} \Delta \nabla \cdot \int_{1000 \text{ hPa}}^{200 \text{ hPa}} q \bar{V}_H dp_{Def-Con}$ ; shaded). **d** Vertical velocity at 500 hPa in m/s. **e** Meridional moisture (shaded, in g/kg) and moisture flux (vectors in  $\text{g/kg} \cdot \text{m/s}$ ) zonally averaged over the shaded region

displayed at the upper right side. Only significant vectors are shown. Figure a–c are in mm/day. Significant changes (t-test,  $p < 0.05$ ) are marked with black slashes. Orography elevation is shown in a–d at 500 and 3500 m a.s.l. as black and grey contours, respectively. The blue line in e represents the Andes' profile calculated as the maximum topographic elevation inside the area displayed in red at the upper right side

shown). Similarly, latent heat flux decreases over regions with evapotranspiration reductions (Figs. 4f, 5b). In the end, the enhanced energy loss through reflected shortwave radiation as well as the reduced incoming longwave radiation flux decrease the surface net radiation over the deforested and surrounding areas (Fig. 4g). This reduction in net radiation is very important for driving alterations in the regional moisture convergence as pointed out by Zeng and Neeling (1999). It is important to remark that the overestimation of the albedo effect and the weaker model responses in sensible heat and longwave outgoing radiation fluxes, as well as roughness length and surface wind velocity (see Sect. 3.2) constrain our conclusions in the following sections.

Figure 5 shows simulated changes in the water balance following Eq. (2). Significant reductions in the seasonal rainfall are found over central and south-western Amazon closely matching the deforestation area (Fig. 5a). To some extent, these precipitation changes are related to the local impact of the decreased evapotranspiration, especially over the center of Brazilian Amazon (Fig. 5b). Nevertheless, for analyzing the effect that evapotranspiration changes induced by deforestation have on rainfall, a quantification of precipitation recycling ratio should be assessed (e.g. Eiras-Barca et al. 2020). On the other hand, the drier conditions over Bolivian Amazon are closely linked with changes in the regional atmospheric circulation, where increased moisture divergence is a response to deforestation (Fig. 5c). Here, the observed northwest-southeast (Fig. 2d) integrated moisture flux at the east of the Andes weakens in the deforested scenario (Fig. 5c). It is interesting to note that near the surface (10 m), an opposite change in the moisture flux enhances the water vapor transport toward the southern and eastern parts of the continent (not shown). This result suggests that in the western Amazon the changes in the vertically integrated

moisture transport are not dominated by the surface conditions; instead, alterations in the integrated humidity transport are related to regional circulation changes such as the decrease in moisture convergence and vertical velocity over most of the Amazon (Fig. 5c, d), the rise in the atmospheric pressure at lower levels (not shown), and a weakening of the regional Hadley cell (Fig. 5e). These changes are in agreement with the theoretical frameworks laid out by Gill (1980) and Eltahir (1996), and with modelling studies (Zhang et al. 1996; Sun and Barros 2015a; Badger and Dirmeyer 2016). Opposite to the forcing in Gill (1980), Amazon deforestation induces a lack of diabatic heating as a result of a drier atmosphere and less convection in the region (Eltahir 1996; Badger and Dirmeyer 2016). This feature is observed in Fig. 5e as a drier troposphere below 650 hPa over 10–18°S and as an enhanced subsidence over the same latitudinal band. These changes are also associated with slightly stronger westerlies at the upper troposphere and a small weakening of the Bolivian High (not shown). Similar changes in the regional circulation and in the regional Hadley cell have been reported by previous modelling and theoretical studies (Zhang et al. 1996; Eltahir 1996; Zeng and Neelin 1999; Badger and Dirmeyer 2016). In the linear model developed by Eltahir (1996), the tropical subsidence is a consequence of a reduction in the boundary layer entropy that follows large-scale deforestation. On the other hand, according to Zeng and Neelin (1999) and in agreement with Fig. 4, reductions in rainfall and moisture convergence over the Amazon basin induced by tropical deforestation can be partially initiated by the enhanced energy loss due to the albedo effect.

On the other hand, Fig. 6 shows the differences between Deforested and Control scenarios for the DJF climatology of the atmospheric stability index, as well as its adiabatic dry and diabatic moist process components following Eq. (3).

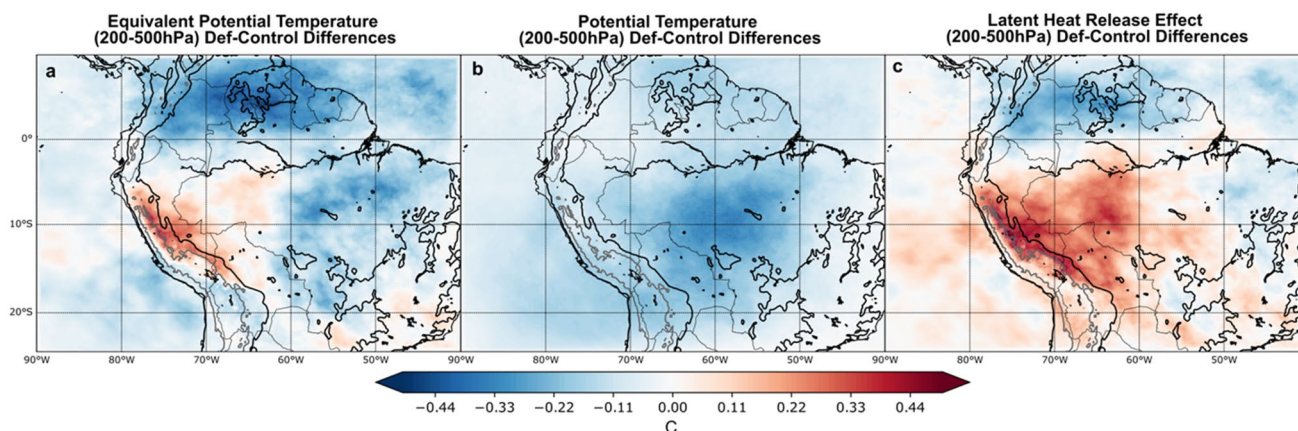


**Fig. 6** DJF seasonal climatological differences Deforested minus Control during 2001–2011 in atmospheric stability index  $\theta_{e(200-500)}$ : **a** Equivalent potential temperature 200 – 500 hPa ( $\Delta\theta_{e(200-500)Def-Con}$ ), **b** Potential temperature 200 – 500 hPa ( $\Delta\theta_{200-500Def-Con}$ ), **c** Latent

heat release effect 200 – 500 hPa ( $\Delta\frac{L_v\theta}{C_p T}_{200-500Def-Con}$ ). All figures are in °C. Orography elevation is shown at 500 and 3500 m a.s.l. as black and grey contours, respectively

An increment in the equivalent potential temperature and the other terms of the equation (red colors in Fig. 6) indicates an increase in the atmospheric stability and an inhibition tendency of the convective activity. Conversely, a decrease in each term of Eq. (3) (blue colors in Fig. 6) implies a reduction trend in atmospheric stability favoring convection development. A first evident result is that dry adiabatic processes exhibit the tendency to reduce the atmospheric stability over the whole region (Fig. 6b). Although with deforestation the troposphere cools at all levels (not shown), the upper levels exhibit a stronger cooling than middle levels, generating the decrease in potential temperature shown in Fig. 6b. This effect is more pronounced over the center of the Brazilian Amazon, near the deforested area. On the contrary, changes in wet processes and latent heat release lead to an increase in the atmospheric stability over the central and western Amazon, including the southern Andes and its eastern foothills (Fig. 6c). It is interesting to highlight that these areas have been recognized to be very sensitive to evapotranspiration upstream of the Amazon basin (Zemp et al. 2017b; Staal et al. 2018). Over the northern and eastern parts of the continent, a decrease in atmospheric stability is related to the enhancement in precipitation and moisture convergence (Fig. 5). Since WRF exhibits an underestimated response in evapotranspiration and latent heat flux to deforestation (Sect. 3.2), the effects in atmospheric stability due to moist diabatic processes could be stronger. Similarly, earlier studies suggested two competing mechanisms as a response of tropical deforestation: (i) a dry atmosphere response linked to warmer surface that increases convergence; (ii) an enhanced divergence leaded by reductions in rainfall and latent heat release (Gill 1980; Lindzen and Nigam 1987; Eltahir and Bras 1993; Eltahir 1996). In summary, our results suggest that the combination of both dry adiabatic and moist (latent heat release) processes produces more stable atmospheric conditions and inhibits precipitation over the western part of the Amazonian basin and the eastern flank of the tropical Andes below the Equator (Fig. 6a). Colombia, Venezuela, Guyana and eastern Brazilian Amazon experience a net reduction in stability and more favorable conditions for convection in the deforested scenario. These alterations are more regional and not limited to deforested areas. Although changes in atmospheric stability are not statistically significant, the 10-year-period analyzed in this work might not be enough for identifying significant differences.

## 4.2 Mesoscale and local changes in daily scale precipitation

The previous section displays how deforestation reduces precipitation and moisture transport, as well as increases the atmospheric stability and inhibits convective activity over the western Amazon and the eastern Andes flank. We analyze the deforestation effect at meso and local scales for

daytime and nighttime conditions over the Amazon-Andes transition region, with a particular focus on the Andean valleys of Huarinilla and Zongo in Bolivia (see Fig. 1 for precise location).

Daytime and nighttime rainfall patterns are shown in Fig. 7 for observations and WRF-D02. During the day, TRMM exhibits high precipitation values over the western part of the Altiplano and Andes highlands (Fig. 7a). Most tropical mountains display this daytime precipitation maximum over summits partially as a result of the thermally driven upslope winds (Garreaud and Wallace 1997; Garreaud 1999; Kikuchi and Wang 2008; Zardi and Whiteman 2013). There are also significant precipitation rates East of the Andes and over Amazonian lowlands during the day as afternoon convection develops (Machado 2002; Romatschke and Houze 2010; Chavez and Takahashi 2017; Fig. 7a). During the night, observed rainfall peaks are located over the eastern Andean piedmonts associated with the so-called rainfall hotspots (Killeen et al. 2007; Halladay et al. 2012; Espinoza et al. 2015; Fig. 7b). This nocturnal convective activity is driven by the convergence of downslope winds from the top of the Andes with the SALLJ nocturnal enhancement (Killeen et al. 2007; Romatschke and Houze 2010; Chavez and Takahashi 2017; Junquas et al. 2018).

In general, WRF-D02 is able to represent the main features of diurnal and nocturnal rainfall variability in the region when compared to TRMM. Rainfall peaks above the 3500 m a.s.l. and over the central Peruvian Altiplano are simulated during the day by WRF as shown in Fig. 7c. Daytime convection over Amazon lowlands below 500 m is also present in WRF outputs in agreement with TRMM. However, the model strongly overestimates daytime precipitation over the Bolivian Amazon plains and over the eastern Andes slopes. Nevertheless, dry biases have been identified by several studies in TRMM outputs over tropical Andes, which makes it difficult to properly quantify the model biases (Condom et al. 2011; Scheel et al. 2011; Rasmussen et al. 2013; Espinoza et al. 2015). During nighttime, WRF realistically represents the rainfall hotspots but exhibits a positive (negative) bias over the Peruvian Andes highlands (Brazilian Amazon lowlands) (Fig. 7d).

Deforestation causes a general rainfall reduction in daytime and nighttime conditions but with different spatial distributions (Fig. 7e, f). During the day, significant precipitation reductions occur over the Amazon plains following the deforested area (between 10 and 20%), but no significant changes occurs over the tropical Andes above 3500 m a.s.l. On the eastern Andean slope between 500 and 3500 m a.s.l., significant changes are found, like in the central Andean-Amazon valleys of Peru near the 10° S and 75° W (Fig. 7e). On the other hand, nighttime convection decrease (between 20 and 30%) is concentrated over the eastern flank of the Andes and particularly over the Bolivian piedmont (Fig. 7f).

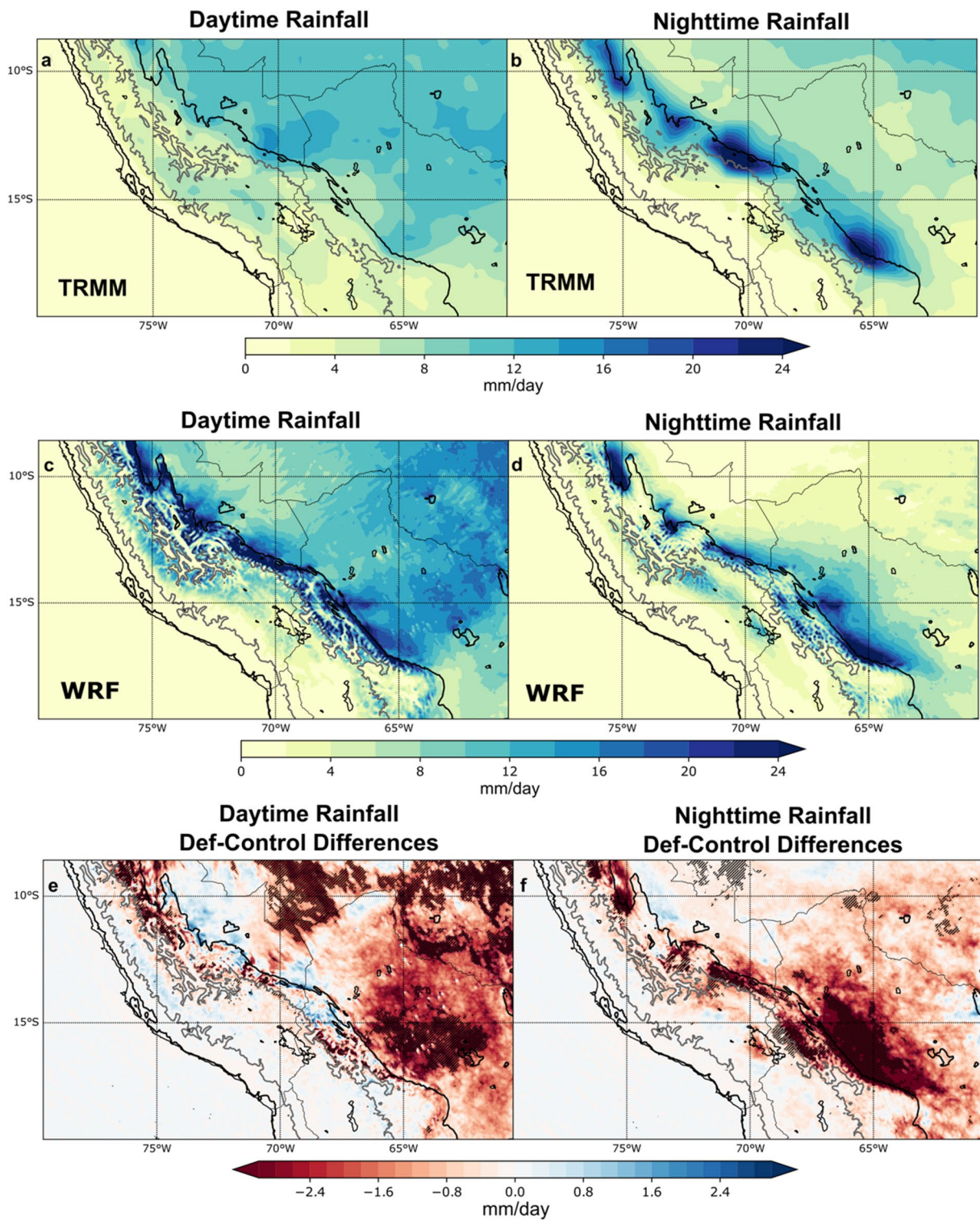


**Fig. 7** DJF climatological means (2001–2011) for daytime and nighttime precipitation from: **a, b** TRMM-3B42. **c, d** WRF-D02. **e, f** WRF-D02 Deforested minus Control differences. All figures are in

mm/day. Significant changes (t-test,  $p < 0.05$ ) are marked with black slashes. Orography elevation is shown at 500 and 3500 m a.s.l. as black and grey contours, respectively

Taking into account that nighttime convection is responsible for nearly the 70–80% of the daily precipitation on the eastern tropical Andes slopes during austral summer (Perry et al. 2014; Chavez and Takahashi 2017), this nocturnal rainfall reduction can have a profound impact in the hydrology of the region. Since nocturnal precipitation over the eastern Andes slopes (including over rainfall hotspots) is closely related to the presence of the SALLJ, in Fig. 8 we evaluate the changes induced by deforestation in the vertically integrated moisture flux over the Bolivian piedmont inside our third modelling domain (Fig. 1). A northwesterly moisture transport is present in both daytime and nighttime conditions during DJF in the Control scenario associated with the SALLJ activity (Fig. 8; e.g. Marengo et al. 2004). This moisture transport is more parallel to the Andes during the day and is stronger and more perpendicular to the slopes during the night in agreement with previous works (Vernekar et al. 2003; Marengo 2004; Junquas et al. 2018; Fig. 8a, b). The humidity flux transported from Amazon toward the Andes is channelized both during day and night over the steepest valleys as modelling and observational works reported in the region (Zängl and Egger 2005; Perry et al. 2014; Junquas et al. 2018; Fig. 8a, b). The Andes act as a blocking barrier

to this moisture laden winds coming from the Amazon lowlands, triggering forced convection mainly during nighttime when the trajectory is more perpendicular to the topography. This mechanism was hypothesized by Espinoza et al. (2015) based on in-situ stations and supported by modelling studies (Junquas et al. 2018).

In the Deforestation scenario, the daytime upslope moisture flux is enhanced over the major valleys (Fig. 8c). However, inside of our region of interest covering Zongo and Huarinilla valleys (black square in Fig. 8) this flux exhibits little changes during the day. Conversely, during the night there is a strong reduction in the humidity transport from the Amazon lowlands towards the Andes highlands over the entire region (Fig. 8d) in agreement with nocturnal rainfall reductions over eastern Andes slopes and Bolivian hotspots shown in Fig. 7f.

During nighttime, we hypothesize that the precipitation and moisture flux depletion in the region is caused by the following process: (i) the atmosphere dries up in the Deforestation scenario over the whole Amazon basin and the northerly moisture flux weakens (Fig. 5); (ii) precipitation decreases over the western Amazon causing less latent heat released to the atmosphere over the region; (iii) there is a

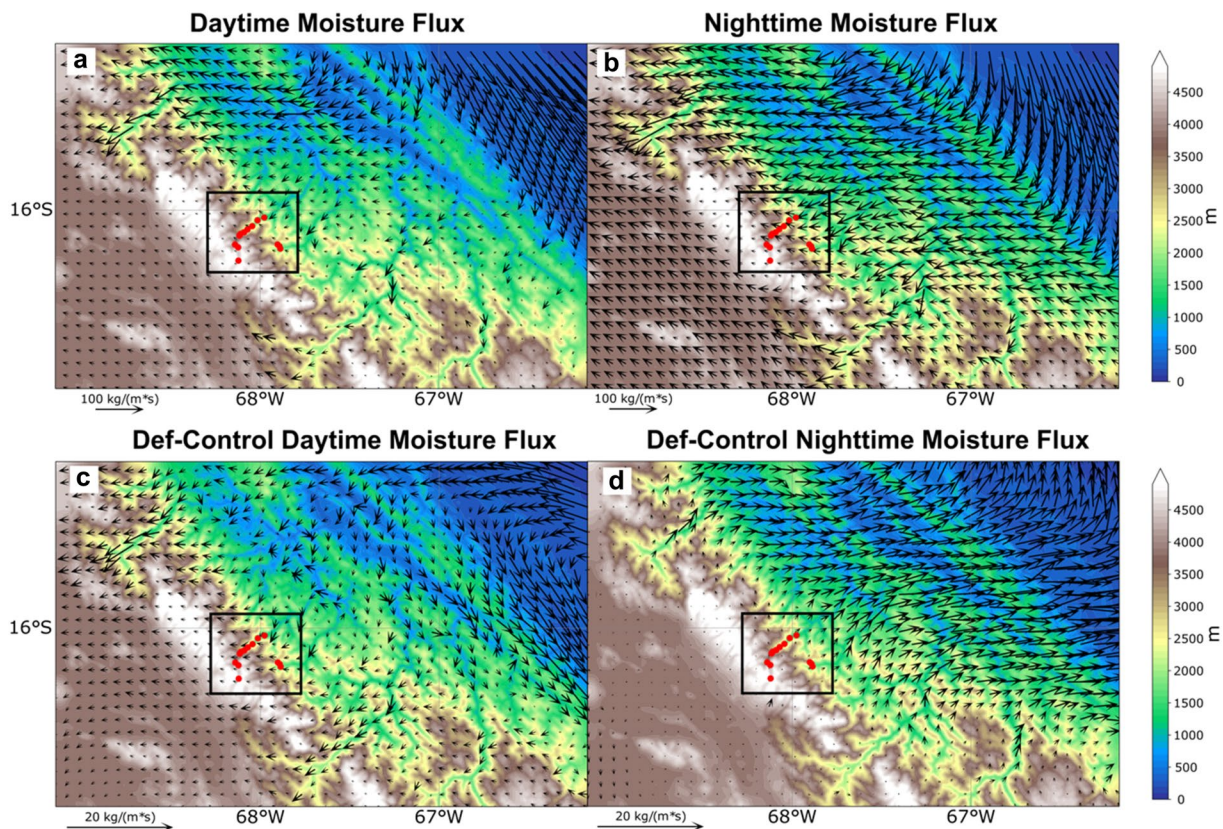


**Fig. 8** DJF climatological means (2001–2011) for daytime and nighttime vertically-integrated moisture flux from WRF-D03: **a, b** Control and **c, d** Deforested minus Control differences. Terrain elevation

in m (shaded) and rain-gauge stations (red dots). The black square shows the area where the Andean valleys of Huarinilla and Zongo are located

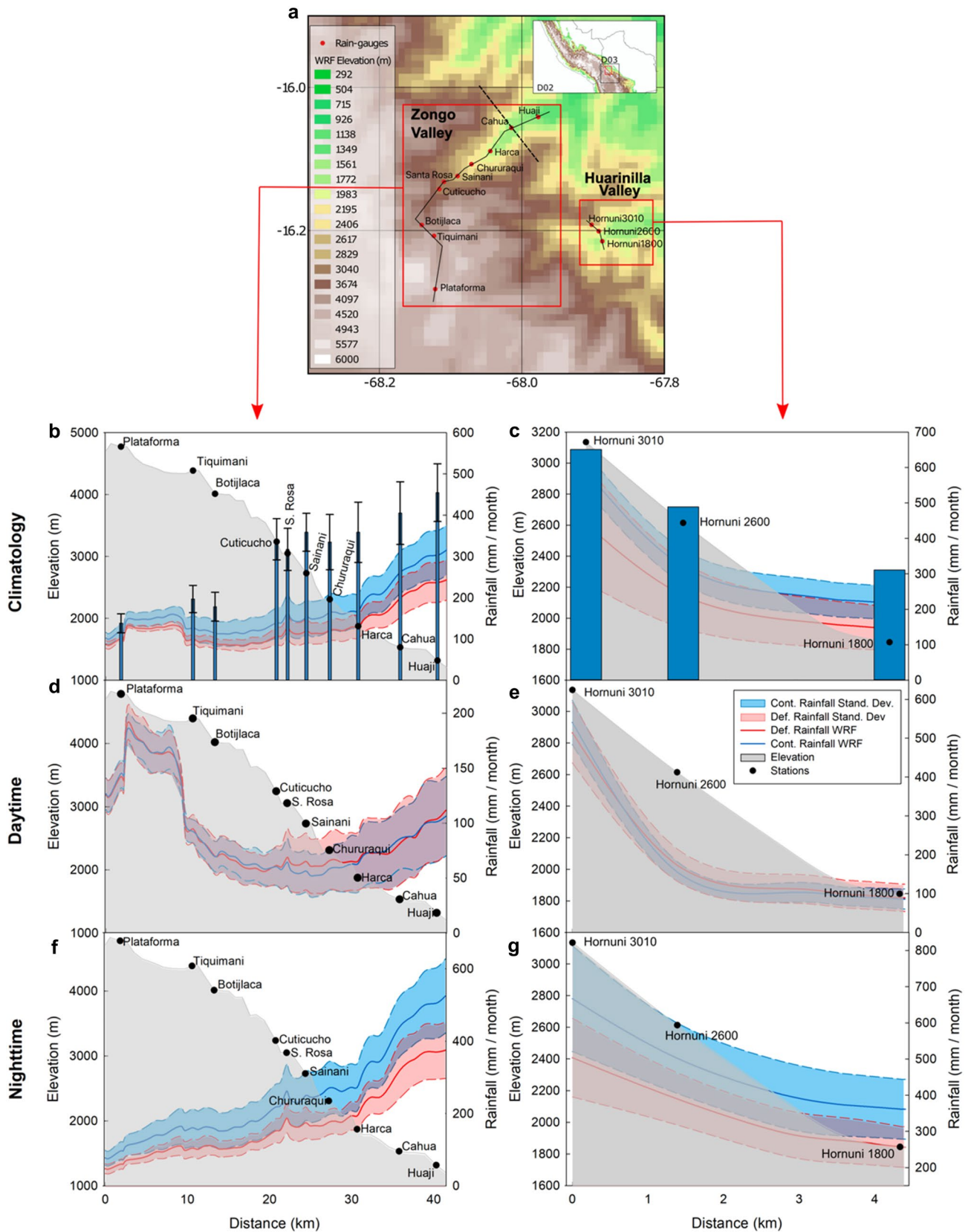




**Fig. 9** **a** Map of the subregion inside D03 with terrain elevation (shaded) in m and rain-gauge stations (red dots). Two selected cross-sections are indicated in black solid lines. A perpendicular cross-section in Zongo Valley shown in Fig. 10 is indicated as a dashed black line. **b, c** Cross-sections for **b** Zongo Valley and **c** Huarinilla Valley. Topographic profiles are displayed as a gray line (in m). Observed rain-gauge rainfall is presented as blue bars. Climatological means for Zongo and Huarinilla valleys corresponds to the periods 2001–2011 and 2001–2002 respectively. WRF-D03 Control and Deforested rainfall 2001–2011 DJF climatological means are shown as blue and red lines and are labeled as Cont. and Def., respectively. **d–g** Same as **b, c** but for daytime and nighttime conditions. Rainfall is in mm/month. The x axis represents the horizontal distance in km along the cross-sections. Blue and red envelopes represent model standard deviation for each scenario. Black dots represent rain-gauge stations

reduction in the local upslope moisture flux over the eastern flank of the Bolivian Andes. By suppressing the condensation latent heating due to rainfall in the Peruvian and Bolivian Andean slopes in a modelling experiment, Junquas et al. (2018) found a positive feedback with the reduction in the entrance of the upslope moisture flux coming from Amazon plains. Since latent heating is more important for sustaining circulation during the night (e.g. Souza et al. 2000), major impacts of such processes happen on nocturnal rainfall. Similarly, by preventing the energy influx into the atmosphere from latent heat fluxes over the eastern flank of the Andes in high resolution climate simulations, Sun and Barros (2015a, b) found a strong reduction in the energy available for moist convection, a decrease in rainfall, moisture convergence and cloudiness in the region, and a weakened upslope flow as a consequence of increased static stability. Our results points towards the same direction: the crucial role of moist processes for sustaining the atmospheric circulation and hydrological condition over the Amazon-Andes transition region.

In order to evaluate the potential impacts of Amazon forest loss on the hydro-climatology at local scales, our analysis is centered in two instrumented valleys located at the eastern flank of the Bolivian Andes: Huarinilla and Zongo valleys (Fig. 9a). The spatial distribution of rain-gauges within the two valleys allows analyzing how precipitation varies with orography and altitude in two opposite directions with respect to the Andean Cordillera. Stations inside the Zongo Valley are located from north-east to south-west in a perpendicular direction to the Andes (Fig. 9a). Conversely, stations located in the Huarinilla Valley are disposed parallel to the mountain chain. Following the rain stations from highlands to lowlands, two cross-sections were defined as shown in black solid lines of Fig. 9a. A third cross-section is analyzed in a perpendicular direction of the Zongo valley (northwest-southeast direction) in order to complement the understanding of local circulation alterations (black dashed line in Fig. 9a). The climatological relationship between precipitation and elevation is shown in Fig. 9b, c. There is an opposite relation between rainfall and terrain elevation in

the two transects. For the Zongo Valley cross-section, precipitation generally decreases with elevation, reaching minimum values above 3000 m a.s.l. and rainfall peaks near the 1000 m a.s.l. (Fig. 9b). This rainfall behavior was previously reported by Espinoza et al. (2015). Chavez and Takahashi (2017) demonstrated how the rainfall change with elevation along cross-sections transversal to the Andes in the region follows the profile of the horizontal moisture flux carried by the SALLJ. In this sense, the rainfall-elevation relation in the first transect seems to be more related with synoptic processes such as the SALLJ and less with local upslope processes in accordance with previous studies (Romatschke and Houze 2010). An opposite behavior is observed in the Huarinilla Valley, where maximum rainfalls are located at high elevations around 3000 m a.s.l. (Fig. 9c). Here, daytime thermally-driven anabatic winds are responsible for transporting moisture transpired inside the valley in the upslope direction and generates a rainfall peak in the afternoon (Molina-Carpio et al. 2019).

WRF exhibits a realistic representation of the rainfall-elevation relationship for both cross-sections. The model reproduces the observed rainfall increases over very local orographic elevations such as the rain-gauges of Tiquimani, Santa Rosa and Sainani. However, a rainfall underestimation (around  $-30\%$ ) occurs in all the stations inside the Zongo Valley and is higher below the 3000 m a.s.l. The model also presents problems in the representation of the steep precipitation decrease that occurs between Cuticucho and Tiquimani and instead exhibits an almost linear rainfall reduction from Huaji to Plataforma. However, this issues in the local variation of precipitation in the Zongo Valley could be related with problems in the representation of local topography. By comparing Table 3 values with Fig. 9, it is easy to identify that for the Zongo Valley, WRF overestimates the real altitude of the stations (from 20 m at Plataforma to 476 m at Sainani). Major differences occur on stations located in places with very high slopes (such as Sainani or Botijlaca). Although our simulations use an enhanced digital elevation model instead of the default dataset in WRF, the complex and steep topography in the region is still poorly represented. This misrepresentation in the local topography can cause issues in the representation of moisture transport, surface circulation and can also affect rainfall and surface air temperature (e.g. Saavedra et al. 2020). On the other hand, taking into account that precipitation is very related to the SALLJ moisture transport in this valley, WRF rainfall underestimation could be related to the weaker SALLJ moisture flux present in the model simulation (not shown). Daytime and nighttime rainfall conditions for both transects are shown in Fig. 9d–g according to WRF outputs. In Zongo Valley, diurnal precipitation is much less than nocturnal values confirming that the dominant mechanism in this valley is the regional moisture transport of the SALLJ (Fig. 9d–f). At

this time, precipitation falls mainly over highlands for both transects as shown in Figs. 9d, e. At the bottom of the Zongo Valley there is a secondary rainfall peak as a consequence of convective activity related with the solar heating over Amazonian plains (Romatsche and Houze 2013). However, in terms of percentage of the summer climatological mean at each station, daytime lowlands rainfall is lower than in the highland. Nighttime rainfall is concentrated mainly at lowlands in agreement with the mechanism described before (Fig. 9f). It is interesting to note that for the Huarinilla Valley, similar precipitation magnitudes are simulated for daytime and nighttime conditions (Fig. 9f, g). This suggests that local and synoptic mechanisms are equally important in this valley as reported from previous works (Molina-Carpio et al. 2019).

Amazon deforestation induces significant reductions in the climatological rainfall mean over both Zongo and Huarinilla cross-sections but increases its interannual variability only in Huarinilla Valley (Fig. 9b, c). Major precipitation drop is located over areas below 2000 m a.s.l. in the Zongo Valley (Fig. 9b). For this cross-section, daytime precipitation presents little changes in its mean value (Fig. 9d). Conversely, during the night precipitation decreases, especially at lowlands, and no change in the variability occurs (Fig. 9f). This result confirms our hypothesis that rainfall depletion in this valley is mainly related with the decreased entry of SALLJ moist winds from Amazon towards the Andes highlands. On the other hand, the Huarinilla Valley cross-section does not present significant changes in daytime rainfall but increases its interannual variability (Fig. 9e). However, decreased rainfall take place during nighttime especially over highlands in agreement with the regional alterations in the SALLJ related moisture flux (Fig. 9g).

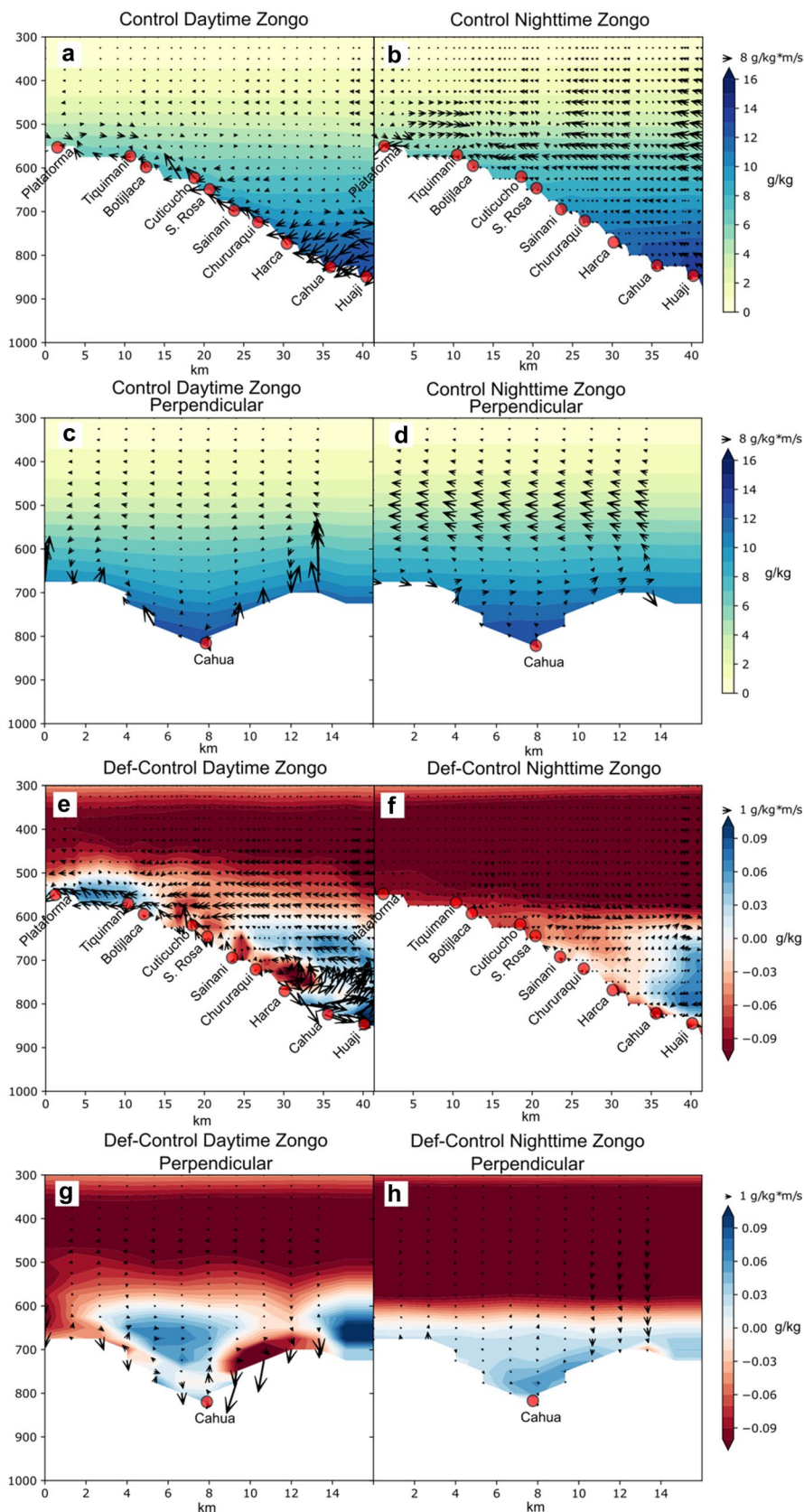
Aiming to complement the previous analysis, Fig. 10 displays the atmospheric humidity and moisture flux in the vertical cross-section along parallel (black solid line in Fig. 9a) and perpendicular (black dashed line in Fig. 9a) directions of the Zongo Valley. Similar results are found for the Huarinilla Valley (not shown). During daytime, upslope moisture flux (Fig. 10a) causes the rainfall peaks over summits described in Fig. 9d. Similar anabatic winds are present in the perpendicular direction of the Zongo Valley (Fig. 10c). During nighttime, surface moisture flux weakens, and light katabatic winds develops in the Zongo Valley (Fig. 10b–d). At the same time, the mid-tropospheric moisture coming from the Amazon plains is strengthened mainly in the perpendicular direction of the Zongo Valley (Fig. 8a, b, 10b–d). Another interesting feature of the nocturnal circulation in the perpendicular direction is the development of a moisture flux around 700 hPa in the opposite direction (northwest-southeast) of the main mid-tropospheric flow (Fig. 10d). This returning flow seems to be a consequence of the ascending motion over lowlands summits to satisfy continuity.

Deforestation induces a weakening of the daytime upslope flow over both directions of the Zongo Valley (Fig. 10e–g). A reduction in the intensity of the daytime circulation increases the atmospheric moisture near the surface at the bottom of the valley (Fig. 10e, g). Based on the thermodynamics of heat engines, Souza et al. (2000) explain the physical mechanism behind the observed circulation over areas with different surface conditions in sloping terrains. According to this work, the intensity of the circulation depends on the absorption of sensible and latent heat by a parcel that moves along a closed streamline. They also recognize the hydrostatic pressure and non-adiabatic expansion/compression as important effects. Following this argument, we assess the surface energy balance along the Zongo Valley for the Control and Deforestation scenarios. We focus on daytime conditions, when local surface heterogeneities play an important role (Fig. 11). However, nighttime changes were also analyzed and are not significant (not shown). Small changes in the incoming shortwave radiation are induced by deforestation in the Zongo Valley and are linked with differences in clouds (Fig. 11a). On the contrary, a strong increment in the reflected shortwave radiation causes a loss of around  $-50 \text{ W/m}^2$  at the bottom of the valley where deforestation occurs (Fig. 11b). The longwave components of the energy balance remain almost unaltered (Fig. 11c, d). Due to the increase in the outgoing shortwave energy loss, the surface net radiation decreases at lowlands below Harca rain-gauge (Fig. 11e). This net radiation reduction generates a decrease in the altitude of the planetary boundary layer (PBL) (Fig. 11f) and is distributed in reductions in latent heat but mainly in sensible heat flux over lowlands (Fig. 11g, h). These fluxes are essential in the triggering and development of upslope flows (e.g., Junquas et al 2018). The reductions in the sensible and latent heat fluxes explain the weakening of the upslope surface circulation during daytime described in Fig. 10. However, these results have to be taken with caution taking into account that WRF strongly underestimates (overestimates) the impact of forest loss on the sensible heat flux (reflected incoming radiation) (Sect. 3.2).

On the other hand, nighttime differences in circulation mainly occur at regional scale through mid-tropospheric moisture flux reduction in the deforested scenario (Figs. 8d, 10f–h). This moisture transport is very important for developing the nocturnal convection and its decrease causes less rainfall over the entire region (Fig. 9f, g). The nighttime conditions are also characterized by a strong reduction in atmospheric humidity above the 600 hPa as a consequence of deforestation (Fig. 10f, h).

Rainfall reductions and increased rainfall variability over Huarinilla and Zongo valleys can impact the wet ecosystems of local humid-montane forest and its endemic biological species (Ibisch et al. 2001; Mueller et al. 2002;

**Fig. 10** Vertical cross-section for daytime and nighttime DJF climatological means (2001–2011) in atmospheric moisture (shaded, g/kg) and moisture flux (vectors, g/kg\*m/s) for the Zongo Valley in two opposite directions: parallel to the transect (see black solid line in Fig. 9a) and perpendicular to the transect (see black dashed line in Fig. 9a). Daytime (a) and nighttime (b) WRF-Control conditions for the transect parallel to the Zongo Valley. Daytime (c) and nighttime (d) WRF-Control conditions for the transect perpendicular to the Zongo Valley. Daytime (e) and nighttime (f) Deforested minus Control differences in the transect parallel to the Zongo Valley. Daytime (g) and nighttime (h) Deforested minus Control differences in the transect perpendicular to the Zongo Valley. Red dots represent rain-gauge stations. Vertical component of the moisture flux is exaggerated by a factor of ten



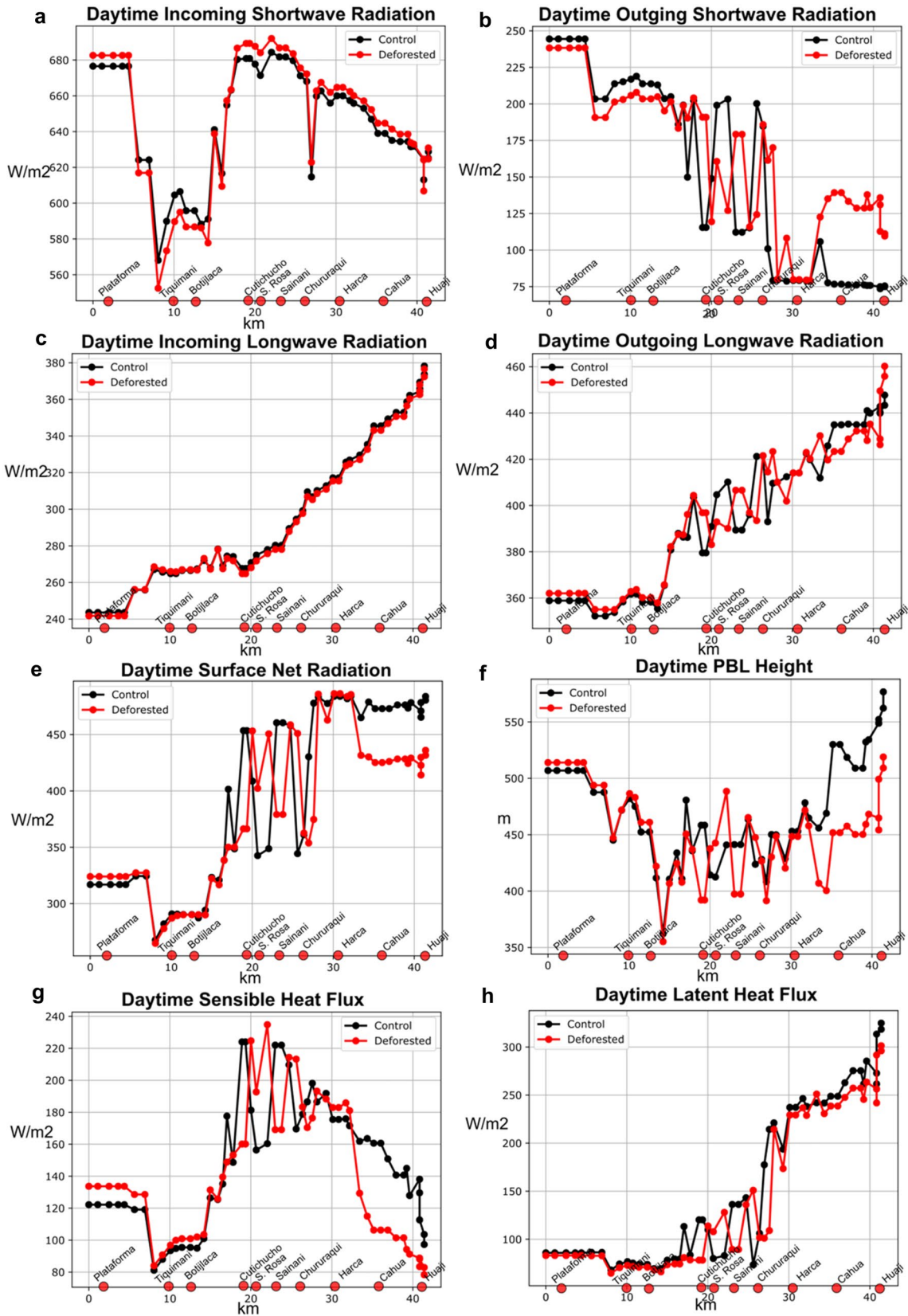


**Fig. 11** WRF-D03 daytime mean variation along the Zongo Valley transect in Control and Deforested scenarios (black and red lines, respectively) for: **a** Shortwave incoming radiation. **b** Shortwave outgoing radiation. **c** Longwave incoming radiation. **d** Longwave outgoing radiation. **e** Surface net radiation. **f** Planetary boundary layer (PBL) height. **g** Sensible heat flux. **h** Latent heat flux. Red dots represent rain-gauge stations

Kessler and Kluge 2008). Additionally, the area encompasses part of the Cordillera Real-Bolivia and the Huayna Potosi Massif where several glaciers (e.g. Zongo Glacier) are located (Francou et al. 1995). The glacier surface mass balance variability of the tropical glaciers is strongly controlled by the precipitation amount and temporal distribution that determine the glacier surface albedo and therefore the surface energy balance (e.g. Sicart et al. 2005; Rabatel et al. 2013), as well as regional atmospheric circulation (Favier et al. 2004; Sicart et al. 2016). Our results state that Amazonian large-scale deforestation can have an important effect in the regional circulation and precipitation. This means that retreat of the tropical Andes glacier documented since the early 1980s and linked to climate change (e.g. Ramírez et al. 2001; Francou et al. 2003; Rabatel et al. 2013) is likely to be further increased as extensive Amazonian deforestation can also have an impact on precipitation and therefore on the surface mass balance of tropical glaciers.

It is important to remark that wide-spread deforestation can have strong nonlocal atmospheric responses (Avisar and Werth 2005; Hasler et al. 2009). Thus, the use of a regional model where both control and deforested scenarios present the same lateral boundary conditions generates a bias where these nonlocal effects are not included (Medvigy et al. 2011). In this sense, the results discussed above do not include the possible remote responses of deforestation in the boundary conditions of our analysis domain. On the other hand, a strong perturbation in the land surface conditions (such as the implementation of a deforestation scenario) can require a long spin-up period for a regional climate model to reach a physical equilibrium state. Surface hydrological variables such as evapotranspiration and soil moisture require long spin-up periods ranging from several months to several years (Christensen 1999; Cosgrove et al. 2003). Since these variables are crucial for surface energy and water budgets, the evaluation of the spin-up window influence in deforestation scenarios is a relevant topic to be evaluated by future studies. Nevertheless, the atmospheric component (which is the main interest in the present study) responds faster to dynamical/thermo-dynamical forcings (de Ela et al. 2002; Cholette et al. 2015; Jerez et al. 2020).

## 5 Summary and conclusions

This study aims to evaluate the impacts of Amazonian deforestation on the hydro-climatic connectivity between Amazon and eastern tropical Andes during the austral summer in terms of hydrological and energetic balances. To this end, we use 10-year December–January–February high-resolution simulations (2001–2011) with the regional climate model WRF. Two scenarios are used: (i) a control simulation corresponding to vegetation conditions for the year 2000; (ii) a business-as-usual deforested scenario (45% of forest lost) designed by Soares-Filho et al. (2006).

By comparing with reanalysis (ERA5 and NCEP-NCAR) and precipitation satellite outputs (TRMM), we find a realistic representation of the main atmospheric circulation (e.g. SALLJ, the Bolivian High) and rainfall features (e.g. SACZ, Amazon convection) during austral summer by WRF at a regional scale. The model is also able to reproduce the daytime and nighttime rainfall conditions over the Amazon-Andes transition region and the rainfall-elevation relation at a local-scales inside instrumented Andean valleys. However, at local scale, in regions with high orography, day and night rainfall conditions were only compared with rain-gauge estimations for a very short period (1 year) in Huarinilla valley. The lack of observations at intra-diurnal time scale in the region is an important limitation for assessing the high-resolution model representation of local atmospheric mechanisms and its interaction with mesoscale features. We complement the validation by assessing the model skill to reproduce the observed land use change impacts on surface fluxes and atmospheric variables at a local scale against LBA stations. We find a realistic model response to deforestation for most of the surface atmospheric variables in Amazon lowlands. However, WRF overestimates the effect of the albedo on the reflected shortwave radiation and strongly underestimates the sensible heat flux and evaporation/latent heat response to forest loss. These model biases constrain our conclusions about the impacts of deforestation on the regional climate. How these errors interact with each other is something that remains unexplored in this work.

At a regional scale, the energy balance is profoundly disrupted by the forest loss. The combined effect of enhanced energy losses through shortwave radiation reflection, longwave incoming and outgoing radiation fluxes leads to a decrease in the surface net radiation over most of the basin. According to the deforestation theory developed by Zeng and Neeling (1998), this reduction in surface net radiation may lead to alterations in the regional moisture convergence. Accordingly, deforestation reduces precipitation almost over the entire Amazonian basin

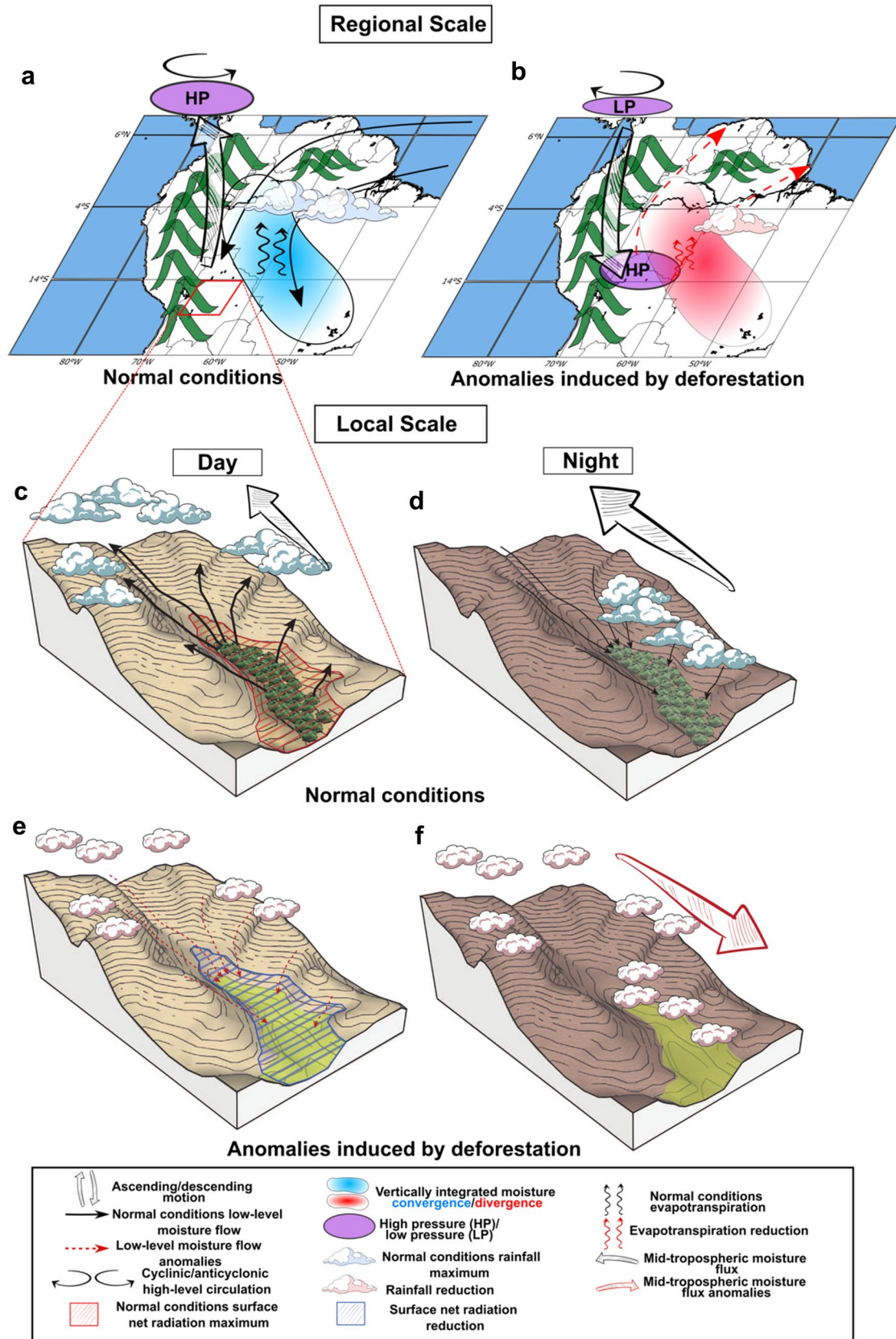


**Fig. 12** Schematic representation of DJF climatological atmospheric conditions at regional (a, b) and local scales (c–f) for normal conditions (a–d) and deforestation induced anomalies (b–f) in WRF simulations. The red square in a indicates the approximated location of the Zongo Valley sketched in c–f. Black solid (red dashed) thin arrows represent surface moisture transport under normal conditions (deforestation anomalies). Black (red) thick arrows represent mid-tropospheric moisture flux under normal conditions (deforestation anomalies). Vertical thick arrows represent ascending and descending motions. Black (red) curved arrows represent evapotranspiration under normal conditions (deforestation anomalies). Blue and red shaded areas indicate vertically integrated moisture convergence and divergence, respectively. Purple areas indicate pressure changes. Blue and red clouds indicate rainfall maximum and rainfall reductions under normal and deforested conditions, respectively. Red (blue) hatched area in c (e) indicates surface net radiation maximum (reduction) under normal (deforestation) conditions

(~20%). Rainfall depletion is related with the very local response of decreased evapotranspiration over cleared areas. The drier atmosphere seems to present a decrease in latent heat release that weakens moisture convergence and causes an anomalous winds subsidence in the region in agreement with early theoretical frameworks. In agreement with these theoretical works, deforestation induces a slight weakening of the Bolivian High and decreases (increases) the 200 hPa geopotential height (surface pressure) over the southwestern Amazon. These alterations in the regional precipitation and atmospheric circulation are summarized in Fig. 12a, b. Regarding the regional atmospheric stability, our analysis suggests the rise of two competing mechanisms for tropical deforestation: (i) an adiabatic response decreases atmospheric stability and enhances convective activity over the continental area; (ii) conversely, reductions in the latent heat release increase atmospheric stability and disfavor convection mainly over western Amazon, and the eastern sides of tropical Andes. Although the effects of deforestation in atmospheric stability are relatively small and non-significant, the underestimated WRF response in latent heat flux to forest loss implies that this effect could be stronger.

Over the Amazon-Andes transition region, deforestation causes a general rainfall reduction in both daytime and nighttime conditions but with a clearly spatial differentiation. Daytime precipitation reductions occur over the Amazon plains following the deforested area (between 10 and 20%). Conversely, nighttime convection decreases between 20 and 30% mainly over the eastern flank of the Andes and over the Bolivian piedmont. Since nighttime convection is responsible for nearly 70–80% of the daily precipitation on the eastern tropical Andes slopes during austral summer, this rainfall reduction can seriously impact the hydrology of the region. The decrease in nocturnal rainfall over eastern Andean hillside is caused by a reduction in the humidity transport from the Amazon

lowlands towards the Andean highlands during nighttime in agreement with previous modelling studies.

Finally, at a local scale, Amazon deforestation induces significant reductions in the climatological rainfall mean over both Zongo and Huarinilla valleys (–25%) and increases its interannual variability. For the Zongo Valley, major precipitation drop occurs over areas below 2000 m a.s.l. In this valley, daytime precipitation presents little changes in its mean value. However, during the night precipitation decreases, especially at lowlands. The rainfall depletion in this valley seems to be mainly related with the decreased entry of SALLJ moist winds from Amazon towards the Andean highlands (Fig. 12d–f). Similarly, the Huarinilla Valley does not present significant changes in daytime rainfall but exhibits decreased precipitation especially over highlands during nighttime. However, as a result of numerical modelling these conclusions have to be taken with caution as they are partially dependent on the model configuration. More efforts have to be done to understand the sensitivity and robustness of these results to model parametrizations. Finally, this work and most of deforestation modelling studies are focused on forest loss impacts on atmospheric processes at climatological time scales. How deforestation can alter rainfall distribution and the atmospheric circulation patterns that drive moisture advection at synoptic intra-seasonal time scale is a question that should be addressed to better understand the deforestation disturbances at longer time scales.

**Supplementary Information** The online version contains supplementary material available at <https://doi.org/10.1007/s00382-021-06025-y>.

**Acknowledgements** We would like to thank Marcus Schawe for providing the rain-gauge data for Hornuni Valley.

**Author contributions** All authors contributed to the study conception and design. Material preparation, data collection and analysis were performed by JPS. The first draft of the manuscript was written by JPS and all authors commented on previous versions of the manuscript. All authors read and approved the final manuscript.

**Funding** This research has been supported by the French AMANECER-MOPGA project funded by ANR and IRD (ref. ANR-18-MPGA-0008). Jorge Molina-Carpio was supported by the Universidad Mayor de San Andres (UMSA) within the framework provided by the PHYBAAM (Processus Hydrologiques des Bassins Andins Amazoniens) Project and HYdrog ochimie du Bassin AMazonien (HYBAM) program.

**Availability of data and material** All dataset sources except WRF modelling results have been properly referenced by showing the source (web site links). The datasets generated during the current study (WRF outputs) are available from the corresponding author on reasonable request.

## Declarations

**Conflict of interest** The authors declare no conflicts of interest or competing interests.

## References

- Alves LM, Marengo JA, Fu R, Bombardi RJ (2017) Sensitivity of Amazon regional climate to deforestation. *Am J Clim Chang*. <https://doi.org/10.4236/ajcc.2017.61005>
- Armijos E, Crave A, Espinoza JC et al (2020) Rainfall control on Amazon sediment flux: synthesis from 20 years of monitoring. *Environ Res Commun* 2:051008. <https://doi.org/10.1088/2515-7620/ab9003>
- Atkinson BW (1989) Meso-scale atmospheric circulations
- Avissar R, Schmidt T (1998) An Evaluation of the scale at which ground-surface heat flux patchiness affects the convective boundary layer using large-eddy simulations. *J Atmos Sci* 55:2666–2689. [https://doi.org/10.1175/1520-0469\(1998\)055%3c2666:AEOTSA%3e2.0.CO;2](https://doi.org/10.1175/1520-0469(1998)055%3c2666:AEOTSA%3e2.0.CO;2)
- Avissar R, Werth D (2005) Global hydroclimatological teleconnections resulting from tropical deforestation. *J Hydrometeorol* 6:134–145. <https://doi.org/10.1175/JHM406.1>
- Badger AM, Dirmeyer PA (2015) Climate response to Amazon forest replacement by heterogeneous crop cover. *Hydrol Earth Syst Sci* 19:4547–4557. <https://doi.org/10.5194/hess-19-4547-2015>
- Badger AM, Dirmeyer PA (2016) Remote tropical and sub-tropical responses to Amazon deforestation. *Clim Dyn* 46:3057–3066. <https://doi.org/10.1007/s00382-015-2752-5>
- Bagley JE, Desai AR, Harding KJ et al (2014) Drought and deforestation: Has land cover change influenced recent precipitation extremes in the Amazon? *J Clim* 27:345–361. <https://doi.org/10.1175/JCLI-D-12-00369.1>
- Bala G, Caldeira K, Wickett M et al (2007) Combined climate and carbon-cycle effects of large-scale deforestation. *Proc Natl Acad Sci USA*. <https://doi.org/10.1073/pnas.0608998104>
- Bastable HG, Shuttleworth WJ, Dallarosa RLG et al (1993) Observations of climate, albedo, and surface radiation over cleared and undisturbed amazonian forest. *Int J Climatol*. <https://doi.org/10.1002/joc.3370130706>
- Berbet MLC, Costa MH (2003) Climate change after tropical deforestation: seasonal variability of surface albedo and its effects on precipitation change. *J Clim* 16:2099–2104. [https://doi.org/10.1175/1520-0442\(2003\)016%3c2099:CCATDS%3e2.0.CO;2](https://doi.org/10.1175/1520-0442(2003)016%3c2099:CCATDS%3e2.0.CO;2)
- Boers N, Marwan N, Barbosa HMJ, Kurths J (2017) A deforestation-induced tipping point for the South American monsoon system. *Sci Rep*. <https://doi.org/10.1038/srep41489>
- Bonan GB (2008) Forests and climate change: forcings, feedbacks, and the climate benefits of forests. *Science* (80–) 320:1444–1449
- Brockhaus P, Lüthi D, Schär C (2008) Aspects of the diurnal cycle in a regional climate model. *Meteorol Zeitschrift* 17:433–443. <https://doi.org/10.1127/0941-2948/2008/0316>
- Brubaker KL, Entekhabi D, Eagleson PS (1993) Estimation of continental precipitation recycling. *J Clim* 6:1077–1089. [https://doi.org/10.1175/1520-0442\(1993\)006%3c1077:EOCPR%3e2.0.CO;2](https://doi.org/10.1175/1520-0442(1993)006%3c1077:EOCPR%3e2.0.CO;2)
- Butt N, De Oliveira PA, Costa MH (2011) Evidence that deforestation affects the onset of the rainy season in Rondonia, Brazil. *J Geophys Res Atmos*. <https://doi.org/10.1029/2010JD015174>
- Chavez SP, Takahashi K (2017) Orographic rainfall hot spots in the Andes-Amazon transition according to the TRMM precipitation radar and in situ data. *J Geophys Res*. <https://doi.org/10.1002/2016JD026282>
- Chen F, Avissar R (1994) Impact of land-surface moisture variability on local shallow convective cumulus and precipitation in large-scale models. *J Appl Meteorol* 33:1382–1401. [https://doi.org/10.1175/1520-0450\(1994\)033%3c1382:IOLSMV%3e2.0.CO;2](https://doi.org/10.1175/1520-0450(1994)033%3c1382:IOLSMV%3e2.0.CO;2)
- Chen F, Dudhia J (2001) Coupling an advanced land surface-hydrology model with the penn state–NCAR MM5 modeling system. Part I: model implementation and sensitivity. *Mon Weather Rev* 129:569–585. [https://doi.org/10.1175/1520-0493\(2001\)129%3c0569:CAALSH%3e2.0.CO;2](https://doi.org/10.1175/1520-0493(2001)129%3c0569:CAALSH%3e2.0.CO;2)
- Cholette M, Laprise R, Thériault J (2015) Perspectives for very high-resolution climate simulations with nested models: illustration of potential in simulating St. Lawrence river valley channelling winds with the fifth-generation canadian regional climate model. *Climate* 3:283–307. <https://doi.org/10.3390/cli3020283>
- Christensen OB (1999) Relaxation of soil variables in a regional climate model. *Tellus A* 51:674–685. <https://doi.org/10.1034/j.1600-0870.1999.00010.x>
- Claussen M, Brovkin V, Ganopolski A (2001) Biophysical versus biogeochemical feedbacks of large-scale land cover change. *Geophys Res Lett*. <https://doi.org/10.1029/2000GL012471>
- Condom T, Rau P, Espinoza JC (2011) Correction of TRMM 3B43 monthly precipitation data over the mountainous areas of Peru during the period 1998–2007. *Hydrol Process* 25:1924–1933. <https://doi.org/10.1002/hyp.7949>
- Correia FWS, Alvalá RCS, Manzi AO (2008) Modeling the impacts of land cover change in Amazonia: a regional climate model (RCM) simulation study. *Theor Appl Climatol* 93:225–244. <https://doi.org/10.1007/s00704-007-0335-z>
- Cosgrove BA, Lohmann D, Mitchell KE et al (2003) Land surface model spin-up behavior in the North American Land Data Assimilation System (NLDAS). *J Geophys Res Atmos*. <https://doi.org/10.1029/2002JD003316>
- Costa MH, Pires GF (2010) Effects of Amazon and Central Brazil deforestation scenarios on the duration of the dry season in the arc of deforestation. *Int J Climatol* 30:1970–1979. <https://doi.org/10.1002/joc.2048>
- D’Almeida C, Vörösmarty CJ, Hurtt GC, Marengo JA, Dingman SL, Keim BD (2007) The effects of deforestation on the hydrological cycle in Amazonia: a review on scale and resolution. *Int J Climatol* 27:633–647. <https://doi.org/10.1002/joc.1475>
- Dalu GA, Pielke RA (1993) Vertical heat fluxes generated by Mesoscale atmospheric flow induced by thermal inhomogeneities in the PBL. *J Atmos Sci* 50:919–926. [https://doi.org/10.1175/1520-0469\(1993\)050%3c0919:VHFGBM%3e2.0.CO;2](https://doi.org/10.1175/1520-0469(1993)050%3c0919:VHFGBM%3e2.0.CO;2)
- de Ela R, Laprise R, Denis B (2002) Forecasting skill limits of nested, limited-area models: a perfect-model approach. *Mon Weather Rev* 130:2006–2023. [https://doi.org/10.1175/1520-0493\(2002\)130%3c2006:FSLONL%3e2.0.CO;2](https://doi.org/10.1175/1520-0493(2002)130%3c2006:FSLONL%3e2.0.CO;2)
- De Noblet-Ducoudré N, Boisier JP, Pitman A et al (2012) Determining robust impacts of land-use-induced land cover changes on surface climate over North America and Eurasia: results from the first set of LUCID experiments. *J Clim*. <https://doi.org/10.1175/JCLI-D-11-00338.1>
- Debortoli NS, Dubreuil V, Hirota M et al (2017) Detecting deforestation impacts in Southern Amazonia rainfall using rain gauges. *Int J Climatol*. <https://doi.org/10.1002/joc.4886>
- Dirmeyer PA, Brubaker KL (2007) Characterization of the global hydrologic cycle from a back-trajectory analysis of atmospheric water vapor. *J Hydrometeorol*. <https://doi.org/10.1175/JHM557.1>
- Dudhia J (1989) Numerical study of convection observed during the winter monsoon experiment using a mesoscale two-dimensional model. *J Atmos Sci* 46:3077–3107. [https://doi.org/10.1175/1520-0469\(1989\)046%3c3077:NSOCOD%3e2.0.CO;2](https://doi.org/10.1175/1520-0469(1989)046%3c3077:NSOCOD%3e2.0.CO;2)
- Duveiller G, Hooker J, Cescatti A (2018) The mark of vegetation change on Earth’s surface energy balance. *Nat Commun* 9:679. <https://doi.org/10.1038/s41467-017-02810-8>



- Egger J, Blacutt L, Ghezzi F et al (2005) Diurnal circulation of the Bolivian Altiplano part I: observations. *Mon Weather Rev* 133:911–924. <https://doi.org/10.1175/MWR2894.1>
- Eiras-Barca J, Dominguez F, Yang Z et al (2020) Changes in South American hydroclimate under projected Amazonian deforestation. *Ann NY Acad Sci*. <https://doi.org/10.1111/nyas.14364>
- Eltahir EAB (1996) Role of vegetation in sustaining large-scale atmospheric circulations in the tropics. *J Geophys Res Atmos* 101:4255–4268. <https://doi.org/10.1029/95JD03632>
- Eltahir EAB, Bras RL (1993) On the response of the tropical atmosphere TIO large-scale deforestation. *Q J R Meteorol Soc* 119:779–793. <https://doi.org/10.1002/qj.49711951209>
- Eltahir EAB, Bras RL (1994) Precipitation recycling in the Amazon basin. *Q J R Meteorol Soc*. <https://doi.org/10.1002/qj.49712051806>
- Espinoza JC, Marengo JA, Ronchail J et al (2014) The extreme 2014 flood in south-western Amazon basin: the role of tropical-subtropical South Atlantic SST gradient. *Environ Res Lett* 9:124007. <https://doi.org/10.1088/1748-9326/9/12/124007>
- Espinoza JC, Chavez S, Ronchail J et al (2015) Rainfall hotspots over the southern tropical Andes: spatial distribution, rainfall intensity, and relations with large-scale atmospheric circulation. *Water Resour Res*. <https://doi.org/10.1002/2014WR016273>
- Espinoza JC, Ronchail J, Marengo JA, Segura H (2019) Contrasting North-South changes in Amazon wet-day and dry-day frequency and related atmospheric features (1981–2017). *Clim Dyn*. <https://doi.org/10.1007/s00382-018-4462-2>
- Espinoza JC, Arias PA, Moron V et al (2021) Recent changes in the atmospheric circulation patterns during the dry-to wet transition season in south tropical South America (1979–2020): impacts on precipitation and fire season. *J Clim*. <https://doi.org/10.1175/JCLI-D-21-0303.1>
- Espinoza Villar JC, Ronchail J, Guyot JL et al (2009) Spatio-temporal rainfall variability in the Amazon basin countries (Brazil, Peru, Bolivia, Colombia, and Ecuador). *Int J Climatol* 29:1574–1594. <https://doi.org/10.1002/joc.1791>
- Farr TG, Rosen PA, Caro E et al (2007) The shuttle radar topography mission. *Rev Geophys*. <https://doi.org/10.1029/2005RG000183>
- Favier V, Wagnon P, Chazarin J-P et al (2004) One-year measurements of surface heat budget on the ablation zone of Antizana Glacier 15, Ecuadorian Andes. *J Geophys Res* 109:D18105. <https://doi.org/10.1029/2003JD004359>
- Fearnside PM (1993) Deforestation in Brazilian Amazonia: the effect of population and land tenure. *Ambio*. [https://doi.org/10.1016/0006-3207\(94\)90222-4](https://doi.org/10.1016/0006-3207(94)90222-4)
- Figueroa SN, Satyamurty P, Da Silva Dias PL (1995) Simulations of the summer circulation over the South American Region with an Eta Coordinate Model. *J Atmos Sci* 52:1573–1584. [https://doi.org/10.1175/1520-0469\(1995\)052%3c1573:SOTSCO%3e2.0.CO;2](https://doi.org/10.1175/1520-0469(1995)052%3c1573:SOTSCO%3e2.0.CO;2)
- Fisher JB, Whittaker RJ, Malhi Y (2011) ET come home: Potential evapotranspiration in geographical ecology. *Glob Ecol Biogeogr* 20:1–18. <https://doi.org/10.1111/j.1466-8238.2010.00578.x>
- Francou B, Ribstein P, Semiond H et al (1995) Balances de glaciers y clima en Bolivia y Peru. *Bull Inst Fr Etudes Andin* 24:661–670
- Francou B, Vuille M, Wagnon P et al (2003) Tropical climate change recorded by a glacier in the central Andes during the last decades of the twentieth century: Chacaltaya, Bolivia, 16°S. *J Geophys Res* 108:4154. <https://doi.org/10.1029/2002JD002959>
- Fu R, Li W (2004) The influence of the land surface on the transition from dry to wet season in Amazonia. *Theor Appl Climatol*. <https://doi.org/10.1007/s00704-004-0046-7>
- Fu R, Yin L, Li W et al (2013) Increased dry-season length over southern Amazonia in recent decades and its implication for future climate projection. *Proc Natl Acad Sci USA*. <https://doi.org/10.1073/pnas.1302584110>
- Garreaud R (1999) Multiscale analysis of the summertime precipitation over the central Andes. *Mon Weather Rev* 127:901–921. [https://doi.org/10.1175/1520-0493\(1999\)127%3c0901:MAOTSP%3e2.0.CO;2](https://doi.org/10.1175/1520-0493(1999)127%3c0901:MAOTSP%3e2.0.CO;2)
- Garreaud R, Wallace JM (1997) The diurnal march of convective cloudiness over the Americas. *Mon Weather Rev* 125:3157–3171. [https://doi.org/10.1175/1520-0493\(1997\)125%3c3157:TDMOCC%3e2.0.CO;2](https://doi.org/10.1175/1520-0493(1997)125%3c3157:TDMOCC%3e2.0.CO;2)
- Gash JHC, Nobre CA (1997) Climatic effects of Amazonian deforestation: some results from ABRACOS. *Bull Am Meteorol Soc* 78:823–830. [https://doi.org/10.1175/1520-0477\(1997\)078%3c0823:CEOADS%3e2.0.CO;2](https://doi.org/10.1175/1520-0477(1997)078%3c0823:CEOADS%3e2.0.CO;2)
- Gash JHC, Shuttleworth WJ (1991) Tropical deforestation: Albedo and the surface-energy balance. *Clim Change* 19:123–133. <https://doi.org/10.1007/BF00142219>
- Gedney N, Valdes PJ (2000) The effect of Amazonian deforestation on the northern hemisphere circulation and climate. *Geophys Res Lett*. <https://doi.org/10.1029/2000GL011794>
- Gill AE (1980) Some simple solutions for heat-induced tropical circulation. *Q J R Meteorol Soc* 106:447–462
- Grell GA, Dévényi D (2002) A generalized approach to parameterizing convection combining ensemble and data assimilation techniques. *Geophys Res Lett* 29:38–1–38–4. <https://doi.org/10.1029/2002GL015311>
- Halladay K, Malhi Y, New M (2012) Cloud frequency climatology at the Andes/Amazon transition: 2. Trends and variability. *J Geophys Res Atmos*. <https://doi.org/10.1029/2012JD017789>
- Hartmann DL, Klein Tank AMG, Rusticucci M, et al (2013) Observations: atmosphere and surface. In: *Climate Change 2013 the Physical Science Basis: Working Group I Contribution to the Fifth Assessment Report of the Intergovernmental Panel on Climate Change*
- Hasler N, Werth D, Avissar R (2009) Effects of tropical deforestation on global hydroclimate: a multimodel ensemble analysis. *J Clim* 22:1124–1141. <https://doi.org/10.1175/2008JCLI2157.1>
- Heredia MB, Junquas C, Prieur C, Condom T (2018) New statistical methods for precipitation bias correction applied to WRF model simulations in the Antisana Region, Ecuador. *J Hydrometeorol* 19:2021–2040. <https://doi.org/10.1175/JHM-D-18-0032.1>
- Hersbach H, Bell B, Berrisford P et al (2020) The ERA5 global reanalysis. *Q J R Meteorol Soc* 146:1999–2049. <https://doi.org/10.1002/qj.3803>
- Hohenegger C, Brockhaus P, Schär C (2008) Towards climate simulations at cloud-resolving scales. *Meteorol Zeitschrift* 17:383–394. <https://doi.org/10.1127/0941-2948/2008/0303>
- Hong S-Y, Noh Y, Dudhia J (2006) A new vertical diffusion package with an explicit treatment of entrainment processes. *Mon Weather Rev* 134:2318–2341. <https://doi.org/10.1175/MWR3199.1>
- Hoorn C, Wesselingh FP, Ter Steege H et al (2010) Amazonia through time: Andean uplift, climate change, landscape evolution, and biodiversity. *Science* (80–) 330:927–931
- Huffman GJ, Bolvin DT, Nelkin EJ et al (2007) The TRMM Multisatellite Precipitation Analysis (TMPA): quasi-global, multiyear, combined-sensor precipitation estimates at fine scales. *J Hydrometeorol* 8:38–55. <https://doi.org/10.1175/JHM560.1>
- Ibisch P, Nowicki C, Müller R (2001) El biocorredor Amorbó-Madidi primeros insumos botánicos para un Plan de Conservación. *Revista de la Sociedad Boliviana de Botánica* 3(1/2):64–103
- Jerez S, López-Romero JM, Turco M et al (2020) On the spin-up period in WRF simulations over Europe: trade-offs between length and seasonality. *J Adv Model Earth Syst*. <https://doi.org/10.1029/2019MS001945>
- Jiménez PA, Dudhia J (2012) Improving the representation of resolved and unresolved topographic effects on surface wind in the WRF

- model. *J Appl Meteorol Climatol* 51:300–316. <https://doi.org/10.1175/JAMC-D-11-084.1>
- Junquas C, Takahashi K, Condom T et al (2018) Understanding the influence of orography on the precipitation diurnal cycle and the associated atmospheric processes in the central Andes. *Clim Dyn*. <https://doi.org/10.1007/s00382-017-3858-8>
- Kalamandeen M, Gloor E, Mitchard E et al (2018) Pervasive rise of small-scale deforestation in Amazonia. *Sci Rep*. <https://doi.org/10.1038/s41598-018-19358-2>
- Kalnay E, Kanamitsu M, Kistler R et al (1996) The NCEP/NCAR 40-year reanalysis project. *Bull Am Meteorol Soc* 77:437–471. [https://doi.org/10.1175/1520-0477\(1996\)077%3c0437:TNYRP%3e2.0.CO;2](https://doi.org/10.1175/1520-0477(1996)077%3c0437:TNYRP%3e2.0.CO;2)
- Kessler M, Kluge J (2008) Diversity and endemism in tropical montane forests—from patterns to processes. *Biodivers Ecol Ser* 2:35–50
- Khanna J, Medvigy D, Fueglistaler S, Walko R (2017) Regional dry-season climate changes due to three decades of Amazonian deforestation. *Nat Clim Chang* 7:200–204. <https://doi.org/10.1038/nclimate3226>
- Kikuchi K, Wang B (2008) Diurnal precipitation regimes in the global tropics\*. *J Clim* 21:2680–2696. <https://doi.org/10.1175/2007JCLI2051.1>
- Killeen TJ, Douglas M, Consiglio T et al (2007) Dry spots and wet spots in the Andean hotspot. *J Biogeogr* 34(8):1357–1373
- Kodama Y (1992) Large-scale common features of subtropical precipitation zones (the Baiu Frontal Zone, the SPCZ, and the SACZ) Part I: characteristics of subtropical frontal zones. *J Meteorol Soc Japan Ser II* 70:813–836. [https://doi.org/10.2151/jmsj1965.70.4\\_813](https://doi.org/10.2151/jmsj1965.70.4_813)
- Lawrence D, Vandeckar K (2015) Effects of tropical deforestation on climate and agriculture. *Nat Clim Chang* 5:27–36. <https://doi.org/10.1038/nclimate2430>
- Lean J, Rowntree PR (1997) Understanding the sensitivity of a GCM Simulation of Amazonian deforestation to the specification of vegetation and soil characteristics. *J Clim* 10:1216–1235. [https://doi.org/10.1175/1520-0442\(1997\)010%3c1216:UTSOAG%3e2.0.CO;2](https://doi.org/10.1175/1520-0442(1997)010%3c1216:UTSOAG%3e2.0.CO;2)
- Lee X, Goulden ML, Hollinger DY et al (2011) Observed increase in local cooling effect of deforestation at higher latitudes. *Nature*. <https://doi.org/10.1038/nature10588>
- Leite-Filho AT, Costa MH, Fu R (2020) The southern Amazon rainy season: the role of deforestation and its interactions with large-scale mechanisms. *Int J Climatol* 40:2328–2341. <https://doi.org/10.1002/joc.6335>
- Lenters JD, Cook KH (1997) On the origin of the Bolivian high and related circulation features of the south American climate. *J Atmos Sci* 54:656–678. [https://doi.org/10.1175/1520-0469\(1997\)054%3c0656:OTOOTB%3e2.0.CO;2](https://doi.org/10.1175/1520-0469(1997)054%3c0656:OTOOTB%3e2.0.CO;2)
- Li W, Fu R (2004) Transition of the large-scale atmospheric and land surface conditions from the dry to the wet season over Amazonia as diagnosed by the ECMWF re-analysis. *J Clim* 17:2637–2651. [https://doi.org/10.1175/1520-0442\(2004\)017%3c2637:TOT-LAA%3e2.0.CO;2](https://doi.org/10.1175/1520-0442(2004)017%3c2637:TOT-LAA%3e2.0.CO;2)
- Li L, Li W, Barros AP (2013) Atmospheric moisture budget and its regulation of the summer precipitation variability over the Southeastern United States. *Clim Dyn* 41:613–631. <https://doi.org/10.1007/s00382-013-1697-9>
- Lin Y-L, Farley RD, Orville HD (1983) Bulk parameterization of the snow field in a Cloud Model. *J Clim Appl Meteorol* 22:1065–1092. [https://doi.org/10.1175/1520-0450\(1983\)022%3c1065:BPOTSF%3e2.0.CO;2](https://doi.org/10.1175/1520-0450(1983)022%3c1065:BPOTSF%3e2.0.CO;2)
- Lindzen RS, Nigam S (1987) On the role of sea surface temperature gradients in forcing low-level winds and convergence in the tropics. *J Atmos Sci* 44:2418–2436. [https://doi.org/10.1175/1520-0469\(1987\)044%3c2418:OTROSS%3e2.0.CO;2](https://doi.org/10.1175/1520-0469(1987)044%3c2418:OTROSS%3e2.0.CO;2)
- Loarie SR, Lobell DB, Asner GP, Field CB (2011) Land-cover and surface water change drive large albedo increases in South America\*. *Earth Interact* 15:1–16. <https://doi.org/10.1175/2010E1342.1>
- Machado LAT (2002) Diurnal march of the convection observed during TRMM-WETAMC/LBA. *J Geophys Res* 107:8064. <https://doi.org/10.1029/2001JD000338>
- Mahowald NM, Ward DS, Doney SC et al (2017) Are the impacts of land use on warming underestimated in climate policy? *Environ Res Lett*. <https://doi.org/10.1088/1748-9326/aa836d>
- Malhi Y, Roberts JT, Betts RA et al (2008) Climate change, deforestation, and the fate of the Amazon. *Science* (80–) 319(5860):169–172
- Marengo JA (2004) Interdecadal variability and trends of rainfall across the Amazon basin. *Theor Appl Climatol*. <https://doi.org/10.1007/s00704-004-0045-8>
- Marengo JA, Tomasella J, Alves LM et al (2011) The drought of 2010 in the context of historical droughts in the Amazon region. *Geophys Res Lett*. <https://doi.org/10.1029/2011GL047436>
- Martinez JA, Dominguez F (2014) Sources of atmospheric moisture for the La Plata River Basin. *J Clim*. <https://doi.org/10.1175/JCLI-D-14-00022.1>
- Medvigy D, Walko RL, Avissar R (2011) Effects of deforestation on spatiotemporal distributions of precipitation in south America. *J Clim* 24:2147–2163. <https://doi.org/10.1175/2010JCLI3882.1>
- Miguez-Macho G, Fan Y (2012) The role of groundwater in the Amazon water cycle: 1. Influence on seasonal streamflow, flooding and wetlands. *J Geophys Res Atmos*. <https://doi.org/10.1029/2012JD017539>
- Mlawer EJ, Taubman SJ, Brown PD et al (1997) Radiative transfer for inhomogeneous atmospheres: RRTM, a validated correlated-k model for the longwave. *J Geophys Res Atmos* 102:16663–16682. <https://doi.org/10.1029/97JD00237>
- Molina-Carpio J, Espinoza D, Coritza E et al (2019) Clima y variabilidad espacial de la ceja de monte y andino húmedo. *Ecol Boliv* 54:40–56
- Moore N, Arima E, Walker R, Ramos da Silva R (2007) Uncertainty and the changing hydroclimatology of the Amazon. *Geophys Res Lett* 34:L14707. <https://doi.org/10.1029/2007GL030157>
- Moquet JS, Crave A, Viers J et al (2011) Chemical weathering and atmospheric/soil CO<sub>2</sub> uptake in the Andean and Foreland Amazon basins. *Chem Geol*. <https://doi.org/10.1016/j.chemgeo.2011.01.005>
- Mourre L, Condom T, Junquas C et al (2016) Spatio-temporal assessment of WRF, TRMM and in situ precipitation data in a tropical mountain environment (Cordillera Blanca, Peru). *Hydrol Earth Syst Sci* 20:125–141. <https://doi.org/10.5194/hess-20-125-2016>
- Mueller R, Beck SG, Lara R (2002) Potential vegetation based on climate-data in the Bolivian Yungas-forests. *Ecol Boliv* 37(2):5–14
- Myers N, Mittermeyer RA, Mittermeyer CG et al (2000) Biodiversity hotspots for conservation priorities. *Nature*. <https://doi.org/10.1038/35002501>
- Nepstad D, Soares-Filho BS, Merry F et al (2009) The end of deforestation in the Brazilian Amazon. *Science* 326:1350–1351. <https://doi.org/10.1126/science.1182108>
- Nobre CA, Sellers PJ, Shukla J (1991) Amazonian deforestation and regional climate change. *J Clim*. [https://doi.org/10.1175/1520-0442\(1991\)004%3c0957:adarcc%3e2.0.co;2](https://doi.org/10.1175/1520-0442(1991)004%3c0957:adarcc%3e2.0.co;2)
- Nobre CA, Sampaio G, Borma LS et al (2016) Land-use and climate change risks in the amazon and the need of a novel sustainable development paradigm. *Proc Natl Acad Sci USA* 113:10759–10768. <https://doi.org/10.1073/pnas.1605516113>
- Oguntuyinbo JS (1970) Reflection coefficient of natural vegetation, crops and urban surfaces in Nigeria. *Q J R Meteorol Soc* 96:430–441. <https://doi.org/10.1002/qj.49709640907>

- Oliver SA, Oliver HR, Wallace JS, Roberts AM (1987) Soil heat flux and temperature variation with vegetation, soil type and climate. *Agric for Meteorol* 39:257–269. [https://doi.org/10.1016/0168-1923\(87\)90042-6](https://doi.org/10.1016/0168-1923(87)90042-6)
- Patton EG, Sullivan PP, Moeng C-H (2005) The Influence of idealized heterogeneity on wet and dry planetary boundary layers coupled to the land surface. *J Atmos Sci* 62:2078–2097. <https://doi.org/10.1175/JAS3465.1>
- Paulson CA (1970) The mathematical representation of wind speed and temperature profiles in the unstable atmospheric surface layer. *J Appl Meteorol* 9:857–861. [https://doi.org/10.1175/1520-0450\(1970\)009%3c0857:TMROWS%3e2.0.CO;2](https://doi.org/10.1175/1520-0450(1970)009%3c0857:TMROWS%3e2.0.CO;2)
- Peixoto J, Oort A (1992) *Physics of climate*. American Institute of Physics, New York, p 520
- Perry LB, Seimon A, Kelly GM (2014) Precipitation delivery in the tropical high Andes of southern Peru: new findings and paleoclimatic implications. *Int J Climatol* 34:197–215. <https://doi.org/10.1002/joc.3679>
- Pielke RAS (1984) Mesoscale meteorological modeling. In: *International Geophysics*, Vol. 78, Academic Press, pp 612
- Pielke RA (2001) Influence of the spatial distribution of vegetation and soils on the prediction of cumulus Convective rainfall. *Rev Geophys* 39:151–177. <https://doi.org/10.1029/1999RG000072>
- Rabatel A, Francou B, Soruco A et al (2013) Current state of glaciers in the tropical Andes: a multi-century perspective on glacier evolution and climate change. *Cryosph* 7:81–102. <https://doi.org/10.5194/tc-7-81-2013>
- Ramírez E, Francou B, Ribstein P et al (2001) Small glaciers disappearing in the tropical Andes: a case-study in Bolivia: Glacier Chacaltaya (16 °S). *J Glaciol* 47:187–194. <https://doi.org/10.3189/172756501781832214>
- Ramos da Silva R, Avissar R (2006) The Hydrometeorology of a deforested region of the Amazon basin. *J Hydrometeorol* 7:1028–1042. <https://doi.org/10.1175/JHM537.1>
- Rasmussen KL, Choi SL, Zuluaga MD, Houze RA (2013) TRMM precipitation bias in extreme storms in South America. *Geophys Res Lett* 40:3457–3461. <https://doi.org/10.1002/grl.50651>
- Rodwell MJ, Hoskins BJ (2001) Subtropical anticyclones and summer monsoons. *J Clim* 14:3192–3211. [https://doi.org/10.1175/1520-0442\(2001\)014%3c3192:SAASM%3e2.0.CO;2](https://doi.org/10.1175/1520-0442(2001)014%3c3192:SAASM%3e2.0.CO;2)
- Romanschke U, Houze RA (2010) Extreme summer convection in South America. *J Clim* 23:3761–3791. <https://doi.org/10.1175/2010JCLI3465.1>
- Ruiz-Vásquez M, Arias PA, Martínez JA, Espinoza JC (2020) Effects of Amazon basin deforestation on regional atmospheric circulation and water vapor transport towards tropical South America. *Clim Dyn*. <https://doi.org/10.1007/s00382-020-05223-4>
- Saad SI, da Rocha HR, Silva Dias MAF, Rosolem R (2010) Can the deforestation breeze change the rainfall in Amazonia? A case study for the BR-163 highway region. *Earth Interact* 14:1–25. <https://doi.org/10.1175/2010EI351.1>
- Saavedra M, Junquas C, Espinoza JC, Silva Y (2020) Impacts of topography and land use changes on the air surface temperature and precipitation over the central Peruvian Andes. *Atmos Res* 234:104711. <https://doi.org/10.1016/j.atmosres.2019.104711>
- Salati E, Vose PB (1984) Amazon Basin: a system in equilibrium. *Science* (80–) 225:129–138. <https://doi.org/10.1126/science.225.4658.129>
- Saleska SR, da Rocha HR, Huete AR et al (2013) LBA-ECO CD-32 flux tower network data compilation, Brazilian Amazon 1999–2006. <https://doi.org/10.3334/ORNDAAC/1174>
- Scala JR, Garstang M, Tao W et al (1990) Cloud draft structure and trace gas transport. *J Geophys Res* 95:17015. <https://doi.org/10.1029/JD095iD10p17015>
- Schawe M, Gerold G, Bach K et al (2011) Hydrometeorological patterns in relation to montane forest types along an elevational gradient in the Yungas of Bolivia. In: *Tropical Montane Cloud Forests*. Cambridge University Press, Cambridge, pp 199–207
- Scheel MLM, Rohrer M, Huggel C et al (2011) Evaluation of TRMM multi-satellite precipitation analysis (TMPA) performance in the Central Andes region and its dependency on spatial and temporal resolution. *Hydrol Earth Syst Sci* 15:2649–2663. <https://doi.org/10.5194/hess-15-2649-2011>
- Segura H, Espinoza JC, Junquas C et al (2020) Recent changes in the precipitation-driving processes over the southern tropical Andes/western Amazon. *Clim Dyn* 54:2613–2631. <https://doi.org/10.1007/s00382-020-05132-6>
- Shuttleworth WJ, Gash JHC, Lloyd CR et al (1984) Eddy correlation measurements of energy partition for Amazonian forest. *Q J R Meteorol Soc* 110:1143–1162. <https://doi.org/10.1002/qj.49711046622>
- Sicart JE, Wagnon P, Ribstein P (2005) Atmospheric controls of the heat balance of Zongo Glacier (16°S, Bolivia). *J Geophys Res* 110:D12106. <https://doi.org/10.1029/2004JD005732>
- Sicart JE, Espinoza JC, Quéno L, Medina M (2016) Radiative properties of clouds over a tropical Bolivian glacier: seasonal variations and relationship with regional atmospheric circulation. *Int J Climatol* 36:3116–3128. <https://doi.org/10.1002/joc.4540>
- Skamarock WC, Klemp JB, Dudhia J, et al (2019) A description of the advanced research WRF model version 4 (No. NCAR/TN-556+STR). <https://doi.org/10.5065/1dfh-6p97>
- Snyder PK (2010) The influence of tropical deforestation on the Northern Hemisphere climate by atmospheric teleconnections. *Earth Interact*. <https://doi.org/10.1175/2010EI280.1>
- Soares-Filho BS, Nepstad DC, Curran LM et al (2006) Modelling conservation in the Amazon basin. *Nature* 440:520–523. <https://doi.org/10.1038/nature04389>
- Souza EP, Renno NO, Dias MAFS (2000) Convective circulations induced by surface heterogeneities. *J Atmos Sci* 57:2915–2922. [https://doi.org/10.1175/1520-0469\(2000\)057%3c2915:CCIBSH%3e2.0.CO;2](https://doi.org/10.1175/1520-0469(2000)057%3c2915:CCIBSH%3e2.0.CO;2)
- Spera SA, Winter JM, Chipman JW (2018) Evaluation of agricultural land cover representations on regional climate model simulations in the Brazilian Cerrado. *J Geophys Res Atmos* 123:5163–5176. <https://doi.org/10.1029/2017JD027989>
- Staal A, Tuinenburg OA, Bosmans JHC et al (2018) Forest-rainfall cascades buffer against drought across the Amazon. *Nat Clim Chang* 8:539–543. <https://doi.org/10.1038/s41558-018-0177-y>
- Stull RB, Ahrens CD (2011) *Meteorology for scientists and engineers*, 3rd edn. Brooks/Cole, Florence, p 924
- Sun X, Barros AP (2015a) Impact of Amazonian evapotranspiration on moisture transport and convection along the eastern flanks of the tropical Andes. *Q J R Meteorol Soc* 141:3325–3343. <https://doi.org/10.1002/qj.2615>
- Sun X, Barros AP (2015b) Isolating the role of surface evapotranspiration on moist convection along the eastern flanks of the tropical Andes using a quasi-idealized approach. *J Atmos Sci* 72:243–261. <https://doi.org/10.1175/JAS-D-14-0048.1>
- Swann ALS, Longo M, Knox RG et al (2015) Future deforestation in the Amazon and consequences for South American climate. *Agric for Meteorol* 214–215:12–24. <https://doi.org/10.1016/j.agrformet.2015.07.006>
- Trachte K (2018) Atmospheric moisture pathways to the highlands of the tropical Andes: Analyzing the effects of spectral nudging on different driving fields for regional climate modeling. *Atmosphere (basel)* 9:456. <https://doi.org/10.3390/atmos9110456>
- Trachte K, Rollenbeck R, Bendix J (2010) Nocturnal convective cloud formation under clear-sky conditions at the eastern Andes of south Ecuador. *J Geophys Res Atmos*. <https://doi.org/10.1029/2010JD014146>

- Van Der Ent RJ, Savenije HHG, Schaeffli B, Steele-Dunne SC (2010) Origin and fate of atmospheric moisture over continents. *Water Resour Res*. <https://doi.org/10.1029/2010WR009127>
- Vauchel P, Santini W, Guyot JL et al (2017) A reassessment of the suspended sediment load in the Madeira River basin from the Andes of Peru and Bolivia to the Amazon River in Brazil, based on 10 years of data from the HYBAM monitoring programme. *J Hydrol*. <https://doi.org/10.1016/j.jhydrol.2017.07.018>
- Vera C, Higgins W, Amador J et al (2006) Toward a unified view of the American monsoon systems. *J Clim* 19:4977–5000. <https://doi.org/10.1175/JCLI3896.1>
- Vernekar AD, Kirtman BP, Fennessy MJ (2003) Low-level jets and their effects on the South American summer climate as simulated by the NCEP Eta model\*. *J Clim* 16:297–311. [https://doi.org/10.1175/1520-0442\(2003\)016%3c0297:LLJATE%3e2.0.CO;2](https://doi.org/10.1175/1520-0442(2003)016%3c0297:LLJATE%3e2.0.CO;2)
- von Randow C, Manzi AO, Kruijt B et al (2004) Comparative measurements and seasonal variations in energy and carbon exchange over forest and pasture in South West Amazonia. *Theor Appl Climatol* 78:5–26. <https://doi.org/10.1007/s00704-004-0041-z>
- Wang H, Fu R (2002) Cross-equatorial flow and seasonal cycle of precipitation over south America. *J Clim* 15:1591–1608. [https://doi.org/10.1175/1520-0442\(2002\)015%3c1591:CEFASC%3e2.0.CO;2](https://doi.org/10.1175/1520-0442(2002)015%3c1591:CEFASC%3e2.0.CO;2)
- Wang J, Bars RL, Eltahir EAB (1996) A stochastic linear theory of mesoscale circulation induced by the thermal heterogeneity of the land surface. *J Atmos Sci* 53:3349–3366. [https://doi.org/10.1175/1520-0469\(1996\)053%3c3349:ASLTOM%3e2.0.CO;2](https://doi.org/10.1175/1520-0469(1996)053%3c3349:ASLTOM%3e2.0.CO;2)
- Wang J, Bras RL, Eltahir EAB (2000) The impact of observed deforestation on the mesoscale distribution of rainfall and clouds in Amazonia. *J Hydrometeorol* 1:267–286. [https://doi.org/10.1175/1525-7541\(2000\)001%3c0267:TIOODO%3e2.0.CO;2](https://doi.org/10.1175/1525-7541(2000)001%3c0267:TIOODO%3e2.0.CO;2)
- Weisman ML, Skamarock WC, Klemp JB (1997) The resolution dependence of explicitly modeled convective systems. *Mon Weather Rev* 125:527–548. [https://doi.org/10.1175/1520-0493\(1997\)125%3c0527:TRDOEM%3e2.0.CO;2](https://doi.org/10.1175/1520-0493(1997)125%3c0527:TRDOEM%3e2.0.CO;2)
- Yang Z, Dominguez F (2019) Investigating land surface effects on the moisture transport over South America with a moisture tagging model. *J Clim* 32:6627–6644. <https://doi.org/10.1175/JCLI-D-18-0700.1>
- Yoon JH, Zeng N (2010) An Atlantic influence on Amazon rainfall. *Clim Dyn*. <https://doi.org/10.1007/s00382-009-0551-6>
- Zängl G, Egger J (2005) Diurnal circulation of the Bolivian Altiplano. Part II: theoretical and model investigations. *Mon Weather Rev* 133:3624–3643. <https://doi.org/10.1175/MWR3033.1>
- Zardi D, Whiteman CD (2013) Diurnal mountain wind systems. Springer Atmospheric Sciences. *Mt Weather Res Forecast*. [https://doi.org/10.1007/978-94-007-4098-3\\_2](https://doi.org/10.1007/978-94-007-4098-3_2)
- Zemp DC, Schleussner CF, Barbosa HMJ et al (2014) On the importance of cascading moisture recycling in South America. *Atmos Chem Phys*. <https://doi.org/10.5194/acp-14-13337-2014>
- Zemp DC, Schleussner C-F, Barbosa HMJ, Rammig A (2017a) Deforestation effects on Amazon forest resilience. *Geophys Res Lett* 44:6182–6190. <https://doi.org/10.1002/2017GL072955>
- Zemp DC, Schleussner CF, Barbosa HMJ et al (2017b) Self-amplified Amazon forest loss due to vegetation-atmosphere feedbacks. *Nat Commun*. <https://doi.org/10.1038/ncomms14681>
- Zeng N, Neelin JD (1999) A land-atmosphere interaction theory for the tropical deforestation problem. *J Clim* 12:857–872. [https://doi.org/10.1175/1520-0442\(1999\)012%3c0857:ALAITF%3e2.0.CO;2](https://doi.org/10.1175/1520-0442(1999)012%3c0857:ALAITF%3e2.0.CO;2)
- Zhang H, McGuffie K, Henderson-Sellers A (1996) Impacts of tropical deforestation. Part II: The role of large-scale dynamics. *J Clim*. [https://doi.org/10.1175/1520-0442\(1996\)009%3c2498:IOTDPI%3e2.0.CO;2](https://doi.org/10.1175/1520-0442(1996)009%3c2498:IOTDPI%3e2.0.CO;2)
- Zhou J, Lau K-M (1998) Does a monsoon climate exist over south America? *J Clim* 11:1020–1040. [https://doi.org/10.1175/1520-0442\(1998\)011%3c1020:DAMCEO%3e2.0.CO;2](https://doi.org/10.1175/1520-0442(1998)011%3c1020:DAMCEO%3e2.0.CO;2)
- Zhuang Y, Fu R, Marengo JA, Wang H (2017) Seasonal variation of shallow-to-deep convection transition and its link to the environmental conditions over the Central Amazon. *J Geophys Res Atmos* 122:2649–2666. <https://doi.org/10.1002/2016JD025993>
- Zubieta R, Getirana A, Espinoza JC, Lavado W (2015) Impacts of satellite-based precipitation datasets on rainfall-runoff modeling of the Western Amazon basin of Peru and Ecuador. *J Hydrol* 528:599–612. <https://doi.org/10.1016/j.jhydrol.2015.06.064>

**Publisher's Note** Springer Nature remains neutral with regard to jurisdictional claims in published maps and institutional affiliations.